

Stability Analysis of Superconducting Electroweak Vortices

Julien Garaud* and Mikhail S. Volkov†

Laboratoire de Mathématiques et Physique Théorique CNRS-UMR 6083,

Université de Tours, Parc de Grandmont, 37200 Tours, FRANCE

We carry out a detailed stability analysis of the superconducting vortex solutions in the Weinberg-Salam theory described in *Nucl.Phys.* **B826** (2010) 174. These vortices are characterized by constant electric current \mathcal{I} and electric charge density I_0 , for $\mathcal{I} \rightarrow 0$ they reduce to Z strings. We consider the generic field fluctuations around the vortex and apply the functional Jacobi criterion to detect the negative modes in the fluctuation operator spectrum. We find such modes and determine their dispersion relation, they turn out to be of two different types, according to their spatial behavior. There are non-periodic in space negative modes, which can contribute to the instability of infinitely long vortices, but they can be eliminated by imposing the periodic boundary conditions along the vortex. There are also periodic negative modes, but their wavelength is always larger than a certain minimal value, so that they cannot be accommodated by the short vortex segments. However, even for the latter there remains one negative mode responsible for the homogeneous expansion instability. This mode may probably be eliminated when the vortex segment is bent into a loop. This suggests that small vortex loops balanced against contraction by the centrifugal force could perhaps be stable.

PACS numbers: 11.15.-q, 11.27.+d, 12.15.-y, 98.80.Cq

*Electronic address: garaud@lmpt.univ-tours.fr

†Electronic address: volkov@lmpt.univ-tours.fr

Contents

I. Introduction	2
II. Superconducting electroweak vortices	5
III. Perturbing the vortex	9
A. Generic perturbation – separation of variables	10
B. Gauge fixing	12
C. Reduction to a Schrödinger problem	14
D. Boundary conditions	15
IV. Stability test	16
A. Jacobi criterion	16
B. Finding the eigenvalue	19
V. Zero current limit	21
VI. Large current limit	25
VII. Charged vortices	28
VIII. Conclusions	35
ACKNOWLEDGEMENTS	37
APPENDIX A. Background field equations	37
APPENDIX B. Perturbation equations	38
References	40

I. INTRODUCTION

Superconducting strings (vortices) were introduced 25 years ago by Witten in the context of a simple field theory model containing two complex scalars and two Abelian vectors

[1]. They generalize the well known Abrikosov-Nielsen-Olesen (ANO) vortex [2] for a non-zero longitudinal current supported by the scalar condensate in the vortex core [3]. The current can be very large, but there is an upper bound for it, which is typical for the superconductivity models, since too large currents produce strong magnetic fields which destroy superconductivity. Witten's superconducting strings have been much studied [3], [4], mainly in the cosmological context [5], [6], since they can be viewed as solutions of some Grand Unification Theory [1] that could perhaps be relevant at the early stages of the cosmological evolution.

The idea that superconducting vortices could also exist in the Weinberg-Salam theory was suggested longtime ago, because this theory, similar to the Witten model, includes scalar and vector fields and admits the 'bare' vortices – Z strings [7]. It was therefore conjectured that it could also have 'dressed Z strings' containing a W condensate in the core [8, 9]. However, when a systematic search of such dressed Z strings gave negative result [10], the whole idea was abandoned for many years. Only very recently it was reconsidered again [11, 12] and it was found that the negative conclusion of Ref. [10] can be circumvented, because it does not actually forbid the superconducting vortices to exist. Such solutions have been explicitly constructed in Refs. [11, 12], but some of their properties turn out to be quite different as compared to those for the Witten strings. In particular, their current can be arbitrarily large, since its increase, although quenching the Higgs condensate, does not destroy superconductivity, because the current is carried by the vector W bosons and not by scalars as in Witten's model.

Superconducting electroweak vortices can be viewed as generalizations of Z strings for non-zero electric current and charge. They exist for any value of the Higgs boson mass and for any weak mixing angle θ_w . Their current I_3 and electric charge density I_0 transform as components of a spacelike vector $I_\alpha = (I_0, I_3)$ under Lorentz boosts along the vortex. The charge can be boosted away by passing to the 'restframe' where the electric field vanishes, while the current never vanishes and can be defined in the Lorentz-invariant way as $\mathcal{I} = \sqrt{I_3^2 - I_0^2}$. The current is supported by the condensate of charged W bosons trapped in the vortex, while outside the vortex the massive fields die away and there remains only the Biot-Savart magnetic field produced by the current. In the $\mathcal{I} \rightarrow 0$ limit the vortices reduce to Z strings. For $\mathcal{I} \gg 1$ they show a large region of size $\sim \mathcal{I}$ where the Higgs field vanishes, and in the very center of this region there is a compact core of size $\sim 1/\mathcal{I}$ containing the

W condensate. In this estimates the unit of \mathcal{I} corresponds to $\sim 10^9$ Amperes, so that the current can typically be quite large. These vortices could perhaps have interesting physical applications, but it is important to clarify their stability properties, which is the subject of the present paper.

The fact that Z strings are unstable [13], [14], [15] does not necessarily mean that their superconducting generalizations should be unstable too. The analysis in the semilocal limit, for $\theta_w = \pi/2$, shows that the current-carrying vortices do possess instabilities, but the corresponding negative modes are all inhomogeneous, with the wavelength always larger than a certain minimal value depending on the current [16]. As a result, all instabilities can be removed by imposing periodic boundary conditions with a sufficiently small period. In this respect the vortex instability is qualitatively similar to the hydrodynamical Plateau-Rayleigh instability of a water jet, or to the Gregory-Lafamme instability of black strings in the theory of gravity in higher dimensions (see [17] for recent reviews).

Below we carry out the stability analysis for the generic superconducting electroweak vortices, for $\theta_w < \pi/2$. We consider the most general field perturbations around the vortex and look for negative modes in the spectrum of the fluctuation operator. Our main conclusions are as follows. For any values of current \mathcal{I} and charge I_0 the vortex possesses inhomogeneous negative modes which can be periodic or non-periodic in space. These instabilities tend, at least as long as the linear perturbation theory applies, to split the vortex into non-uniform fragments. However, imposing the periodic boundary conditions with a period L along the vortex will remove all non-periodic negative modes. In addition, if L is small enough, all inhomogeneous periodic negative modes will be removed as well, similarly to what one finds in the semilocal limit [16]. Although this suggests that the periodic vortex segments should be stable [12], they still possess the *homogeneous* perturbation mode, which is not removed by periodic boundary conditions, since it can be viewed as periodic with any period. It is therefore important to know whether this mode is negative or not. It is actually non-negative for any \mathcal{I} if $\theta_w = \pi/2$, and for any θ_w if $\mathcal{I} = 0$, in which cases the periodic vortex segments can be stable. However, the detailed analysis reveals that for generic θ_w, \mathcal{I} the homogeneous mode is negative, so that the vortices remain unstable even after imposing the periodic boundary conditions. The instability makes them grow thicker.

At the same time, it is possible that this remaining instability can be removed if the vortex segment is bent and its ends are identified to make a loop, since the thickness of a loop with

a fixed radius cannot grow indefinitely. It is therefore possible that loops made of vortex pieces and balanced against contraction by the centrifugal force arising from the momentum circulating along them could perhaps be stable. This conjecture can be considered as the ‘positive’ outcome of our analysis. Of course, its verification requires serious efforts, since one has to explicitly construct spinning vortex loops and then study their stability. However, any possibility to have stable electroweak solitons can be very important.

The rest of the paper is organized as follows. In Sec.II the electroweak field equations are introduced and their vortex solutions are described. Sec.III considers the generic vortex perturbations, separation of variables in the perturbation equations, gauge fixing, and reduction to a multi-channel Schrödinger problem. Sec.IV describes the Jacobi criterion used to reveal the existence of negative modes in the perturbation operator spectrum, as well as the explicit construction of these modes. The limits of zero current and large current are considered, respectively, in Sec.V and Sec.VI. The electrically charged vortices are discussed in Sec.VII, while Sec.VIII contains concluding remarks. The two Appendices list the complete equations for the background fields and for their perturbations.

II. SUPERCONDUCTING ELECTROWEAK VORTICES

The bosonic sector of the Weinberg-Salam theory is determined by the action density

$$\mathcal{L} = -\frac{1}{4g^2} W_{\mu\nu}^a W^{a\mu\nu} - \frac{1}{4g'^2} B_{\mu\nu} B^{\mu\nu} + (D_\mu \Phi)^\dagger D^\mu \Phi - \frac{\beta}{8} (\Phi^\dagger \Phi - 1)^2. \quad (2.1)$$

Here the Higgs field $\Phi^{\text{tr}} = (\Phi_1, \Phi_2)$ is in the fundamental representation of SU(2), its covariant derivative is $D_\mu \Phi = (\partial_\mu - \frac{i}{2} B_\mu - \frac{i}{2} \tau^a W_\mu^a) \Phi$ with τ^a being the Pauli matrices, while the field strengths are $W_{\mu\nu}^a = \partial_\mu W_\nu^a - \partial_\nu W_\mu^a + \epsilon_{abc} W_\mu^b W_\nu^c$ and $B_{\mu\nu} = \partial_\mu B_\nu - \partial_\nu B_\mu$. The two coupling constants are $g = \cos \theta_w$ and $g' = \sin \theta_w$ where the physical value of the weak mixing angle is $\sin^2 \theta_w = 0.23$. All quantities in (2.1) are rendered dimensionless by rescaling, their dimensionfull analogues (written in boldface) being $\mathbf{B}_\mu = \Phi_0 B_\mu$, $\mathbf{W}_\mu^a = \Phi_0 W_\mu^a$, $\Phi = \Phi_0 \Phi$, the spacetime coordinates $\mathbf{x}^\mu = x^\mu / \mathbf{g}_0 \Phi_0$. Here Φ_0 is the Higgs field vacuum expectation value and \mathbf{g}_0 relates to the electron charge via $\mathbf{e} = gg' \hbar c \mathbf{g}_0$.

The theory is invariant under the SU(2)×U(1) gauge transformations

$$\Phi \rightarrow U\Phi, \quad \mathcal{W} \rightarrow U\mathcal{W}U^{-1} + 2iU\partial_\mu U^{-1}dx^\mu, \quad (2.2)$$

with $U = \exp\left(\frac{i}{2}\vartheta + \frac{i}{2}\tau^a\theta^a\right)$ where ϑ, θ^a are functions of x^μ and $\mathcal{W} = (B_\mu + \tau^a W_\mu^a)dx^\mu$ is the $SU(2)\times U(1)$ Lie-algebra valued gauge field. Varying the action with respect to the fields gives the field equations,

$$\partial^\mu B_{\mu\nu} = g'^2 \frac{i}{2} ((D_\nu\Phi)^\dagger\Phi - \Phi^\dagger D_\nu\Phi), \quad (2.3)$$

$$D^\mu W_{\mu\nu}^a = g^2 \frac{i}{2} ((D_\nu\Phi)^\dagger\tau^a\Phi - \Phi^\dagger\tau^a D_\nu\Phi), \quad (2.4)$$

$$D_\mu D^\mu\Phi + \frac{\beta}{4}(\Phi^\dagger\Phi - 1)\Phi = 0, \quad (2.5)$$

with $D_\mu W_{\alpha\beta}^a = \partial_\mu W_{\alpha\beta}^a + \epsilon_{abc}W_\mu^b W_{\alpha\beta}^c$.

The perturbative mass spectrum of the theory contains the photon and the massive Z, W and Higgs bosons with masses, respectively, being $m_Z = 1/\sqrt{2}$, $m_W = gm_Z$, $m_H = \sqrt{\beta}m_Z$ (in units of $e\Phi_0/(gg')$). The exact value of the parameter β is currently unknown, but it is constraint to belong to the interval $1.5 \leq \beta \leq 3.5$. Defining the electromagnetic and Z fields as [18]

$$F_{\mu\nu} = \frac{g}{g'} B_{\mu\nu} - \frac{g'}{g} n^a W_{\mu\nu}^a, \quad Z_{\mu\nu} = B_{\mu\nu} + n^a W_{\mu\nu}^a \quad (2.6)$$

with $n^a = \Phi^\dagger\tau^a\Phi/(\Phi^\dagger\Phi)$ the electromagnetic current density is

$$J_\mu = \partial^\nu F_{\nu\mu}. \quad (2.7)$$

A straight vortex oriented along the x^3 axis can be described by splitting the spacetime coordinates x^μ into two groups: $x^k = (x^1, x^2)$ spanning the 2-planes orthogonal to the vortex, and $x^\alpha = (x^0, x^3)$ parameterizing the ‘vortex worldsheet’. Introducing the worldsheet vectors

$$\Sigma_\alpha = (\sinh(b), \cosh(b)), \quad \tilde{\Sigma}_\alpha = (\cosh(b), \sinh(b)), \quad \sigma_\alpha = \sigma\Sigma_\alpha, \quad (2.8)$$

with b, σ being two parameters, one makes the stationary, cylindrically symmetric field ansatz [12]

$$\begin{aligned} \mathcal{W} = & u(\rho)\sigma_\alpha dx^\alpha - v(\rho)d\varphi + \tau^1 [u_1(\rho)\sigma_\alpha dx^\alpha - v_1(\rho)d\varphi] \\ & + \tau^3 [u_3(\rho)\sigma_\alpha dx^\alpha - v_3(\rho)d\varphi], \quad \Phi = \begin{pmatrix} f_1(\rho) \\ f_2(\rho) \end{pmatrix}, \end{aligned} \quad (2.9)$$

where $f_1, f_2 \in \mathbb{R}$ and the polar coordinates are introduced, $x^1 + ix^2 = \rho e^{i\varphi}$. In what follows we shall call b, σ , respectively, the boost and twist parameters. This ansatz keeps its form under Lorentz boosts along the x^3 axis whose only effect is to shift the value of b . This

parameter is thus purely cinematic – one can always pass to the ‘restframe’ where $b = 0$ and the field configuration is purely magnetic. The ansatz (2.9) also keeps its form under gauge transformations (2.2) generated by $U = \exp\{-\frac{i}{2}\Gamma\tau^2\}$ with constant Γ , whose effect is

$$(f_1 + if_2) \rightarrow e^{\frac{i}{2}\Gamma}(f_1 + if_2), \quad (u_1 + iu_3) \rightarrow e^{-i\Gamma}(u_1 + iu_3), \quad (v_1 + iv_3) \rightarrow e^{-i\Gamma}(v_1 + iv_3). \quad (2.10)$$

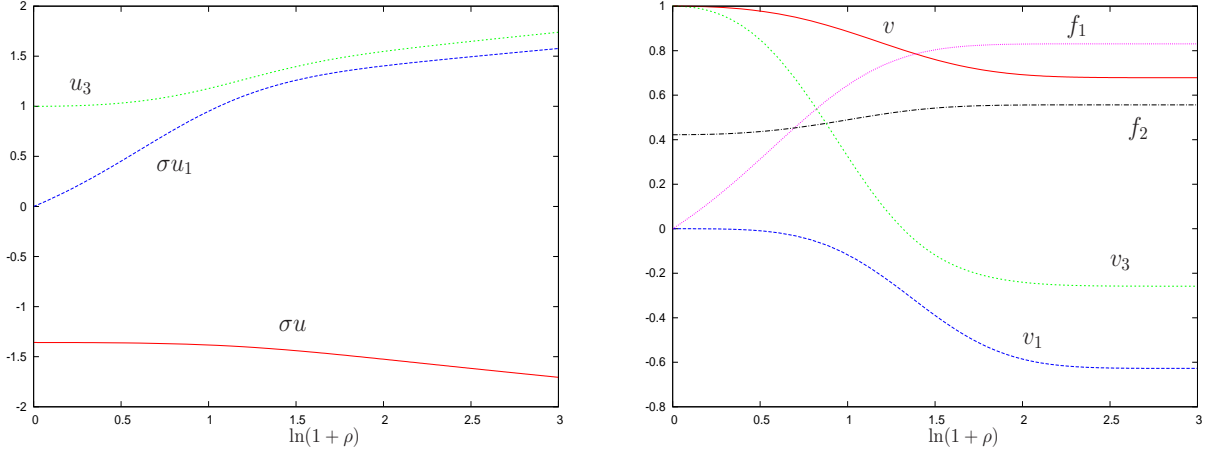


Figure 1: Profile functions for the vortex solution with $\mathcal{I} = 2.57$, $n = \nu = 1$, $\beta = 2$, $\sin^2 \theta_W = 0.23$.

With the parametrization (2.9) the field equations (2.3)–(2.5) reduce to a system of ordinary differential equations (A.1)–(A.9) for the eight functions $u, u_1, u_3, v, v_1, v_3, f_1, f_2$ listed in the Appendix A. It is worth noting that the boost parameter b drops from these equations, but they explicitly depend on the twist parameter σ . The boundary conditions for the equations are obtained by requiring the energy density to be finite and the fields to approach at large ρ the purely electromagnetic Biot-Savart solution associated with the infinitely long electric wire. The local analysis in the vicinity of $\rho = 0, \infty$ then gives the following boundary conditions for the field amplitudes for $0 \leftarrow \rho \rightarrow \infty$ (keeping only the leading terms) [12]

$$\begin{aligned} a_1 \leftarrow u &\rightarrow c_1 + Q \ln \rho, & 2n - \nu \leftarrow v &\rightarrow c_2, \\ 0 \leftarrow u_1 &\rightarrow -(c_1 + Q \ln \rho) \sin \gamma, & 0 \leftarrow v_1 &\rightarrow -c_2 \sin \gamma, \\ 1 \leftarrow u_3 &\rightarrow -(c_1 + Q \ln \rho) \cos \gamma, & \nu \leftarrow v_3 &\rightarrow -c_2 \cos \gamma, \\ 0 \leftarrow f_1 &\rightarrow \cos \frac{\gamma}{2}, & q \delta_n^\nu \leftarrow f_2 &\rightarrow \sin \frac{\gamma}{2}, \end{aligned} \quad (2.11)$$

where $a_1, c_1, c_2, Q, \gamma, q$ are real while n, ν are integers. These boundary conditions imply in fact that the vector fields (2.9) are singular at the symmetry axis, but this singularity can

be removed by the gauge transformation (2.2) with $U = e^{i(n-\nu/2)\varphi} e^{i\nu\varphi\tau^3/2}$ which renders all fields φ -dependent,

$$\begin{aligned} \mathcal{W} = & \{u(\rho) + \tau_\varphi u_1(\rho) + \tau^3 u_3(\rho)\} \sigma_\alpha dx^\alpha \\ & + \{2n - \nu - v(\rho) - \tau_\varphi v_1(\rho) + \tau^3 [\nu - v_3(\rho)]\} d\varphi, \quad \Phi = \begin{bmatrix} e^{in\varphi} f_1(\rho) \\ e^{i(n-\nu)\varphi} f_2(\rho) \end{bmatrix} \end{aligned} \quad (2.12)$$

where $\tau_\varphi = \tau^1 \cos(\nu\varphi) - \tau^2 \sin(\nu\varphi)$. The logarithmically growing at large ρ terms in the solutions is the specialty of the Biot-Savart field, which is essentially the Coulombian potential in two dimensions. The local analysis also shows [12] that the fields approach their asymptotics (2.11) for $\rho \rightarrow \infty$ exponentially fast as $e^{-m_H\rho}$, $e^{-m_Z\rho}$, $e^{-m_\sigma\rho}$ where $m_\sigma = \sqrt{m_W^2 + \sigma^2 u(\rho)^2}$ is the W-boson mass ‘dressed’ by the interaction with the long-range Biot-Savart field.

Numerically integrating Eqs.(A.1)–(A.8) with the boundary conditions (2.11) gives the global solutions in the interval $\rho \in [0, \infty)$ [12]. These solutions can be viewed as field-theoretic realizations of electric wires, where the wire is represented by a regular distribution of massive non-linear fields in the vortex core, while in the far field zone the massive fields die away and everything reduces to the pure Biot-Savart field.

The vortices have the winding number $n \geq 1$ and the ‘polarization’ index $\nu = 1, 2, \dots, \nu_{\max}$ where $\nu_{\max}(\beta, \theta_w, n)$ ranges from n for $\theta_w = \pi/2$ to $2n - 1$ for $\theta_w = 0$. In addition, they are characterized by the worldsheet current vector

$$I_\alpha = \int \partial^\mu F_{\mu\alpha} d^2x = -\frac{2\pi Q \sigma_\alpha}{gg'} \equiv \mathcal{I} \Sigma_\alpha. \quad (2.13)$$

Here $I_0 = \mathcal{I} \sinh(b)$ is the electric charge per unit vortex length and $I_3 = \mathcal{I} \cosh(b)$ is the total electric current through the vortex cross section. It is convenient to use \mathcal{I}, b instead of I_α as the solution parameters.

The typical profiles of the solutions are shown in Fig.1. When $\mathcal{I} \rightarrow 0$ these solutions reduce to Z strings, that is to the embedded ANO vortices. For $\mathcal{I} \neq 0$ the amplitudes u, u_1, u_3 grow with ρ and show the logarithmic tails at infinity. Solutions up to $\mathcal{I} \approx 12$ were constructed in Ref.[12], and since the dimensionless value $\mathcal{I} = 1$ corresponds to $c\Phi_0 = 1.8 \times 10^9$ Amperes, the vortex current can in fact be quite large. In addition, it seems that there is no upper bound for possible values of \mathcal{I} , at least in the classical theory. This can probably be related to the fact that the vortex current is carried by the vector W bosons demonstrating the anti-screening effect [19] – the W condensate sets up currents which tend to increase the magnetic field and not decrease it as in the conventional Meissner effect.

When considered in the restframe, where $b = I_0 = 0$, the vortex is purely magnetic and characterized by its current \mathcal{I} and the magnetic and Z fluxes. Charged (boosted) vortices with $I_0 \neq 0$ have in addition the electric field, momentum and angular momentum.

III. PERTURBING THE VORTEX

Let us consider small perturbations around the vortex configuration (W_μ^a, B_μ, Φ) ,

$$W_\mu^a \rightarrow W_\mu^a + \delta W_\mu^a, \quad B_\mu \rightarrow B_\mu + \delta B_\mu, \quad \Phi \rightarrow \Phi + \delta\Phi. \quad (3.14)$$

Inserting this into the equations (2.3)–(2.5) and linearizing with respect to $\delta W_\mu^a, \delta B_\mu, \delta\Phi$ gives the perturbation equations

$$\begin{aligned} D_\mu D^\mu \delta\Phi - i(\delta B_\mu + \delta W_\mu^a \tau^a) D^\mu \Phi + \frac{\beta}{4}(2|\Phi|^2 - 1)\delta\Phi + \frac{\beta}{4}\delta\Phi^\dagger \Phi^2 \\ = \frac{i}{2}(\partial_\mu \delta B^\mu + \tau^a \mathcal{D}_\mu \delta W^{a\mu})\Phi, \end{aligned} \quad (3.15a)$$

$$\begin{aligned} \partial_\mu \partial^\mu \delta B^\nu + \frac{g'^2}{2}\{\Phi^\dagger(\delta B^\nu + \delta W^{a\nu} \tau^a)\Phi + 2i(\delta\Phi^\dagger D^\nu \Phi - (D^\nu \Phi)\delta\Phi)\} \\ = \partial^\nu \left(\partial_\mu \delta B^\mu + \frac{ig'^2}{2}(\delta\Phi^\dagger \Phi - \Phi^\dagger \delta\Phi) \right), \end{aligned} \quad (3.15b)$$

$$\begin{aligned} \mathcal{D}_\mu \mathcal{D}^\mu \delta W^{a\nu} + \epsilon_{abc} \delta W_\mu^b W^{c\mu\nu} \\ + \frac{g^2}{2}\{\Phi^\dagger \tau^a \delta\Phi(\delta B^\nu + \delta W^{c\nu} \delta_c^a) + 2i(\delta\Phi^\dagger \tau^a D^\nu \Phi - (D^\nu \Phi)\tau^a \delta\Phi)\} \\ = \mathcal{D}^\nu \left(\mathcal{D}_\mu \delta W^{a\mu} + \frac{ig^2}{2}(\delta\Phi^\dagger \tau^a \Phi - \Phi^\dagger \tau^a \delta\Phi) \right), \end{aligned} \quad (3.15c)$$

with $\mathcal{D}_\mu X^a \equiv \partial_\mu X^a + \epsilon_{abc} W_\mu^b X^c$.

These equations are invariant under the infinitesimal gauge transformations,

$$\delta\Phi \rightarrow \delta\Phi + \frac{i}{2}(\delta\vartheta + \delta\theta^a \tau^a)\Phi, \quad \delta B_\mu \rightarrow \delta B_\mu + \partial_\mu \delta\vartheta, \quad \delta W_\mu^a \rightarrow \delta W_\mu^a + \mathcal{D}_\mu \delta\theta^a. \quad (3.16)$$

To suppress the pure gauge modes, we impose the background gauge conditions,

$$\begin{aligned} \partial_\mu \delta B^\mu + \frac{ig'^2}{2}(\delta\Phi^\dagger \Phi - \Phi^\dagger \delta\Phi) = 0, \\ \mathcal{D}_\mu \delta W^{a\mu} + \frac{ig^2}{2}(\delta\Phi^\dagger \tau^a \Phi - \Phi^\dagger \tau^a \delta\Phi) = 0, \end{aligned} \quad (3.17)$$

which eliminates the right hand sides in Eqs.(3.15b),(3.15c). However, this still leaves the residual gauge freedom generated by parameters which fulfill the ghost equations (n^a being

defined after (2.6))

$$\begin{aligned} \partial_\mu \partial^\mu \delta\vartheta + \frac{g'^2}{2} \Phi^\dagger \Phi (\delta\vartheta + n^a \delta\theta^a) &= 0, \\ \mathcal{D}_\mu \mathcal{D}^\mu \delta\theta^a + \frac{g^2}{2} \Phi^\dagger \Phi (n^a \delta\vartheta + \delta\theta^a) &= 0. \end{aligned} \quad (3.18)$$

A. Generic perturbation – separation of variables

Since the background fields depend only on the radial coordinate ρ , we can Fourier-decompose the perturbations with respect to x^α, φ . Keeping in mind the action of the Lorentz boosts on the background solutions, we wish to keep track of their action on the perturbations too. We therefore introduce $\Xi \equiv (\omega \tilde{\Sigma}_\alpha + \kappa \Sigma_\alpha) x^\alpha + m\varphi$, which reduces in the restframe to $\omega x^0 + \kappa x^3 + m\varphi$. Denoting $\delta W_\mu^0 \equiv \delta B_\mu$ the generic perturbations can be decomposed as

$$\begin{aligned} \delta\Phi_a &= \sum_{\omega, \kappa, m} \{ [\phi_a(\omega, \kappa, m|\rho) + i\psi_a(\omega, \kappa, m|\rho)] \cos \Xi \\ &\quad + [\pi_a(\omega, \kappa, m|\rho) + i\chi_a(\omega, \kappa, m|\rho)] \sin \Xi \} , \\ -\delta W_\mu^a \tilde{\Sigma}^\mu &= \sum_{\omega, \kappa, m} \{ X_1^a(\omega, \kappa, m|\rho) \cos \Xi + Y_1^a(\omega, \kappa, m|\rho) \sin \Xi \} , \\ -\delta W_\mu^a \Sigma^\mu &= \sum_{\omega, \kappa, m} \{ X_4^a(\omega, \kappa, m|\rho) \cos \Xi + Y_4^a(\omega, \kappa, m|\rho) \sin \Xi \} , \\ \delta W_k^a &= \sum_{\omega, \kappa, m} \{ X_k^a(\omega, \kappa, m, \rho) \cos \Xi + Y_k^a(\omega, \kappa, m, \rho) \sin \Xi \} , \end{aligned} \quad (3.19)$$

where $a = 1, 2$ and $k = 1, 2$ while now $a = 0, 1, 2, 3$. The infinitesimal gauge transformations Eq.(3.16) can be decomposed in the same way (with $\theta^0 \equiv \vartheta$)

$$\delta\theta^a = \sum_{\omega, \kappa, m} \{ \alpha^a(\omega, \kappa, m|\rho) \cos \Xi + \gamma^a(\omega, \kappa, m|\rho) \sin \Xi \} . \quad (3.20)$$

Inserting the decompositions (3.19) into Eqs.(3.15) the variables x^α, φ decouple and one obtains, for given ω, κ, m , a system of 40 ordinary differential equations for the 40 radial functions ϕ_a, \dots, Y_k^a in (3.19). These 40 equations split (if $\kappa \in \mathbb{R}$) into 2 independent subsystem of 20 equations each. These subsystems are identical to each other upon the

replacement

$$\begin{aligned}
\pi_a &\leftrightarrow \phi_a, & \psi_a &\leftrightarrow -\chi_a, \\
Y_k^a &\leftrightarrow X_k^a, & Y_2^2 &\leftrightarrow X_2^2, \\
X_2^a &\leftrightarrow -Y_2^a, & X_k^2 &\leftrightarrow -Y_k^2.
\end{aligned} \tag{3.21}$$

Here $a = 1, 2$ but $a = 0, 1, 3$ and $k = 1, 3, 4$ (where possible we shall not write explicitly the arguments $(\omega, \kappa, m|\rho)$). Such a splitting of the equations into two groups is the consequence of the fact that the background configurations (2.9) are *real*, and so that the real and imaginary parts of their perturbations should be independent. In Sec.VII below we shall study the case of complex κ, ω , and then the 40 equations do not split into two subsystems any more, but for the time being κ is real and we can restrict our analysis to the 20 equations. These are equations for the 20 radial amplitudes in the right hand sides of (3.21), they factorize with $\cos \Xi$.

These equations are rather long and we do not write them down explicitly. Not all of them are independent, since there are four identities relating them to each other. These are the linearized versions of the identities obtained by taking the divergences of the vector field equations (2.3) and (2.4), their existence is the manifestation of the gauge invariance. The equations are also invariant under the action of the gauge transformations, which now assume the following explicit form:

$$\begin{aligned}
X_1^0 &\rightarrow X_1^0 - \omega \gamma^0, & X_1^1 &\rightarrow X_1^1 - \omega \gamma^1, \\
Y_2^0 &\rightarrow Y_2^0 + (\gamma^0)', & Y_2^1 &\rightarrow Y_2^1 + (\gamma^1)', \\
X_3^0 &\rightarrow X_3^0 + m \gamma^0, & X_3^1 &\rightarrow X_3^1 + m \gamma^1 + v_3 \alpha^2, \\
X_4^0 &\rightarrow X_4^0 + \kappa \gamma^0, & X_4^1 &\rightarrow X_4^1 + \kappa \gamma^1 - \sigma u_3 \alpha^2, \\
Y_1^2 &\rightarrow Y_1^2 + \omega \alpha^2, & X_1^3 &\rightarrow X_1^3 - \omega \gamma^3, \\
X_2^2 &\rightarrow X_2^2 + (\alpha^2)', & Y_2^3 &\rightarrow Y_2^3 + (\gamma^3)', \\
Y_3^2 &\rightarrow Y_3^2 - m \alpha^2 + (v_1 \gamma^3 - v_3 \gamma^1), & X_3^3 &\rightarrow X_3^3 + m \gamma^3 - v_1 \alpha^2, \\
Y_4^2 &\rightarrow Y_4^2 - \kappa \alpha^2 + \sigma(u_3 \gamma^1 - u_1 \gamma^3), & X_4^3 &\rightarrow X_4^3 + \kappa \gamma^3 + \sigma u_1 \alpha^2, \\
\phi_1 &\rightarrow \phi_1 + \frac{1}{2} \alpha^2 f_2, & \chi_1 &\rightarrow \chi_1 + \frac{1}{2} [(\gamma^0 + \gamma^3) f_1 + \gamma^1 f_2], \\
\phi_2 &\rightarrow \phi_2 - \frac{1}{2} \alpha^2 f_1, & \chi_2 &\rightarrow \chi_2 + \frac{1}{2} [\gamma^1 f_1 + (\gamma^0 - \gamma^3) f_2],
\end{aligned} \tag{3.22}$$

where the prime denotes differentiation with respect to ρ .

B. Gauge fixing

The additional terms on the right in (3.22) are pure gauge modes. They automatically fulfill the perturbation equations for any gauge functions $\gamma^0 \equiv \gamma^0(\omega, \kappa, m|\rho), \gamma^1, \alpha^2, \gamma^3$ (verification of this is a good consistency check). We need to impose gauge conditions to eliminate these non-physical solutions. For example, one can use the temporal gauge, which completely eliminates all gauge degrees of freedom [16]. However, the fluctuation operator becomes then rather complicated. We have therefore chosen to use the background gauge conditions (3.17), they lead to more easy to handle equations, although not eliminating completely all gauge modes.

After separating the variables the background gauge conditions (3.17) reduce to four constraint equations

$$\begin{aligned}
\omega X_1^0 - \left(\partial_\rho + \frac{1}{\rho} \right) Y_2^0 + \frac{m}{\rho^2} X_3^0 + \kappa X_4^0 + g'^2 (f_1 \chi_1 + f_2 \chi_2) &= 0, \\
\omega X_1^1 - \left(\partial_\rho + \frac{1}{\rho} \right) Y_2^1 + \frac{m}{\rho^2} X_3^1 + \kappa X_4^1 + g^2 (f_2 \chi_1 + f_1 \chi_2) + \sigma u_3 Y_4^2 - \frac{v_3}{\rho^2} Y_3^2 &= 0, \\
-\omega Y_1^2 - \left(\partial_\rho + \frac{1}{\rho} \right) X_2^2 - \frac{m}{\rho^2} Y_3^2 - \kappa Y_4^2 + g^2 (f_2 \phi_1 - f_1 \phi_2) \\
+ \sigma (u_1 X_4^3 - u_3 X_4^1) + \frac{1}{\rho^2} (v_3 X_3^1 - v_1 X_3^3) &= 0, \\
\omega X_1^3 - \left(\partial_\rho + \frac{1}{\rho} \right) Y_2^3 + \frac{m}{\rho^2} X_3^3 + \kappa X_4^3 + g^2 (f_1 \chi_1 - f_2 \chi_2) - \sigma u_1 Y_4^2 + \frac{v_1}{\rho^2} Y_3^2 &= 0. \quad (3.23)
\end{aligned}$$

Imposing these, one discovers that the 20 radial equations split into two independent subsystems as 4+16, since the four amplitudes in (3.23) which are proportional to ω decouple from the remaining 16 amplitudes. Let us call these four amplitudes temporal, they are governed by the equations

$$\begin{pmatrix} D_1 & S & 0 & T \\ S & D_2 & U & W \\ 0 & U & D_3 & V \\ T & W & V & D_4 \end{pmatrix} \begin{pmatrix} X_1^0/g' \\ X_1^1/g \\ Y_1^2/g \\ X_1^3/g \end{pmatrix} = 0, \quad (3.24)$$

where

$$\begin{aligned}
D_1 &= -\frac{1}{\rho}\partial_\rho(\rho\partial_\rho) + \frac{m^2}{\rho^2} + \kappa^2 - \omega^2 + \frac{g'^2}{2}(f_1^2 + f_2^2), \\
D_2 &= -\frac{1}{\rho}\partial_\rho(\rho\partial_\rho) + \frac{m^2 + v_3^2}{\rho^2}\sigma^2 u_3^2 + \kappa^2 - \omega^2 + \frac{g^2}{2}(f_1^2 + f_2^2), \\
D_3 &= -\frac{1}{\rho}\partial_\rho(\rho\partial_\rho) + \frac{m^2 + v_1^2 + v_3^2}{\rho^2}\sigma^2(u_1^2 + u_3^2) + \kappa^2 - \omega^2 + \frac{g^2}{2}(f_1^2 + f_2^2), \\
D_4 &= -\frac{1}{\rho}\partial_\rho(\rho\partial_\rho) + \frac{m^2 + v_1^2}{\rho^2}\sigma^2 u_1^2 + \kappa^2 - \omega^2 + \frac{g^2}{2}(f_1^2 + f_2^2),
\end{aligned} \tag{3.25}$$

and the off-diagonal terms are

$$\begin{aligned}
S &= gg' f_1 f_2, & T &= gg'(f_1^2 - f_2^2), \\
U &= -2\left(\frac{mv_3}{\rho^2} + \kappa\sigma u_3\right), & V &= -2\left(\frac{mv_1}{\rho^2} - \kappa\sigma u_1\right), & W &= -\left(\frac{v_1 v_3}{\rho^2} + \sigma^2 u_1 u_3\right).
\end{aligned} \tag{3.26}$$

A direct verification reveals that if one resolves the constraints (3.23) with respect to the temporal amplitudes, then the temporal equations will be automatically fulfilled by virtue of the equations for the remaining 16 amplitudes. The latter are described by Eqs.(3.30) below. Every solution of the 16-channel problem (3.30) therefore generates a solution of the temporal equations (3.24). This can be understood by noting that the temporal equations coincide with the ghost equations.

The ghost equations describe the residual gauge freedom left in the background gauge. They can be obtained by inserting the pure gauge modes in (3.22) into (3.23), or equivalently injecting the mode decomposition (3.20) into (3.18). This gives four radial equations for the gauge parameters $\gamma^0, \gamma^1, \alpha^2, \gamma^3$ which coincide with the temporal equations (3.24) upon the replacement

$$X_1^0 \leftrightarrow \gamma^0, \quad X_1^1 \leftrightarrow \gamma^1, \quad Y_1^2 \leftrightarrow -\alpha^2, \quad X_1^3 \leftrightarrow \gamma^3. \tag{3.27}$$

Therefore, the temporal amplitudes are pure gauge modes. It follows that they can be constructed via resolving the constraints (3.23) if only the corresponding solutions of (3.30) are also pure gauge. Resolving the constraints for a non-pure gauge solution of (3.30) should also give a solution of the temporal equations (3.24), but since it cannot then be pure gauge, it can only be trivial. This gives a simple recipe to distinguish between the physical and unphysical solutions of the 16-channel Schrödinger system (3.30): if a solution fulfills the constraints (3.23) with zero temporal amplitudes then it is non-trivial, otherwise it is pure gauge.

We have explicitly tested this recipe for the negative modes of the system (3.30). These modes are all physical, since the spectrum of the ghost operator is positive, and because they fulfill the constraints (3.23) with $X_1^0 = X_1^1 = Y_1^2 = X_1^3 = 0$.

Since the four temporal amplitudes vanish for the physical solutions, one can use the constraints (3.23) in order to algebraically express four other amplitudes (for example those proportional to κ) in terms of the remaining 12 amplitudes. The system (3.30) then reduces to 12 independent equations only, which coincide with the equations obtained in the temporal gauge. However, their structure turns out to be rather complicated, which is why we prefer to work with the 16-channel system (3.30).

C. Reduction to a Schrödinger problem

Imposing the background gauge conditions decouples the 4 temporal/ghost amplitudes, while the equations for the remaining 16 amplitudes can be cast into a Schrödinger form after the following operations. We redefine the amplitudes as

$$\begin{aligned}
Y_2^0 &= \frac{g'}{\sqrt{2}} \left(\frac{g'}{g} (\mathcal{Z}_+ + \mathcal{Z}_-) + \mathcal{A}_+ + \mathcal{A}_- \right), & Y_2^3 &= \frac{1}{\sqrt{2}} (g (\mathcal{Z}_+ + \mathcal{Z}_-) - g' (\mathcal{A}_+ + \mathcal{A}_-)), \\
X_3^0 &= g' \frac{\rho}{\sqrt{2}} \left(\frac{g'}{g} (\mathcal{Z}_+ - \mathcal{Z}_-) + \mathcal{A}_+ - \mathcal{A}_- \right), & X_3^3 &= \frac{\rho}{\sqrt{2}} (g (\mathcal{Z}_+ - \mathcal{Z}_-) - g' (\mathcal{A}_+ - \mathcal{A}_-)), \\
X_4^0 &= g' \left(\frac{g'}{g} \mathcal{Z}_0 + \mathcal{A}_0 \right), & X_4^3 &= (g \mathcal{Z}_0 - g' \mathcal{A}_0), \\
Y_2^1 &= \frac{1}{2} (\mathcal{W}_+^+ + \mathcal{W}_+^- + \mathcal{W}_-^+ + \mathcal{W}_-^-), & X_2^2 &= \frac{1}{2} (\mathcal{W}_+^+ + \mathcal{W}_+^- - \mathcal{W}_-^+ - \mathcal{W}_-^-), \\
X_3^1 &= \frac{\rho}{2} (\mathcal{W}_+^+ - \mathcal{W}_+^- + \mathcal{W}_-^+ - \mathcal{W}_-^-), & Y_3^2 &= \frac{\rho}{2} (-\mathcal{W}_+^+ + \mathcal{W}_+^- + \mathcal{W}_-^+ - \mathcal{W}_-^-), \\
X_4^1 &= \frac{1}{\sqrt{2}} (\mathcal{W}_0^- + \mathcal{W}_0^+), & Y_4^2 &= \frac{1}{\sqrt{2}} (\mathcal{W}_0^- - \mathcal{W}_0^+), \\
\phi_1 &= \frac{1}{2g} (h_1^- - h_1^+), & \chi_1 &= \frac{1}{2g} (h_1^- + h_1^+), \\
\phi_2 &= \frac{1}{2g} (h_2^- - h_2^+), & \chi_2 &= \frac{1}{2g} (h_2^- + h_2^+). \tag{3.28}
\end{aligned}$$

Here the notation \mathcal{A} , \mathcal{Z} and \mathcal{W}^\pm reflect the fact that these amplitudes correspond to the photon, Z and W bosons, respectively. The subscripts refer to their polarizations. Introducing the 16-component vector

$$\Psi^{\text{tr}} = (\mathcal{Z}_0, \mathcal{Z}_+, \mathcal{Z}_-, \mathcal{A}_0, \mathcal{A}_+, \mathcal{A}_-, \mathcal{W}_0^+, \mathcal{W}_+^+, \mathcal{W}_-^+, \mathcal{W}_0^-, \mathcal{W}_+^-, \mathcal{W}_-^-, h_1^+, h_1^-, h_2^+, h_2^-), \tag{3.29}$$

the equations assume the form

$$-\frac{1}{\rho}(\rho\Psi')' + \mathcal{U}(\kappa, m|\rho)\Psi = \omega^2\Psi, \quad (3.30)$$

where \mathcal{U} is a 16×16 symmetric potential energy matrix depending on the background fields. Its explicit form is given in the Appendix B. These equations are invariant under $\omega \rightarrow -\omega$, $\kappa \rightarrow -\kappa$ and $m \rightarrow -m$ provided that

$$\begin{aligned} \mathcal{Z}_0(\omega, \kappa, m|\rho) &\rightarrow -\mathcal{Z}_0(-\omega, -\kappa, -m|\rho), & \mathcal{Z}_\pm(\omega, \kappa, m|\rho) &\rightarrow \mathcal{Z}_\mp(-\omega, -\kappa, -m|\rho), \\ \mathcal{A}_0(\omega, \kappa, m|\rho) &\rightarrow -\mathcal{A}_0(-\omega, -\kappa, -m|\rho), & \mathcal{A}_\pm(\omega, \kappa, m|\rho) &\rightarrow \mathcal{A}_\mp(-\omega, -\kappa, -m|\rho), \\ \mathcal{W}_0^\pm(\omega, \kappa, m|\rho) &\rightarrow -\mathcal{W}_0^\mp(-\omega, -\kappa, -m|\rho), & \mathcal{W}_\pm^\pm(\omega, \kappa, m|\rho) &\rightarrow \mathcal{W}_\mp^\mp(-\omega, -\kappa, -m|\rho), \\ h_a^\pm(\omega, \kappa, m|\rho) &\rightarrow h_a^\mp(-\omega, -\kappa, -m|\rho). \end{aligned} \quad (3.31)$$

D. Boundary conditions

The small ρ behavior of the perturbations can be determined by solving Eqs.(3.30) in power series. For each of the 16 equations we find two solutions, one of which is bounded for $\rho \rightarrow 0$ while the other one is divergent. The bounded solutions are

$$\begin{aligned} \mathcal{Z}_\eta &= c_\eta^Z \rho^{|m-\eta|} + \dots, & \mathcal{A}_\eta &= c_\eta^A \rho^{|m-\eta|} + \dots, & \mathcal{W}_\eta^\pm &= c_\eta^{W^\pm} \rho^{|\nu^\pm(m-\eta)|} + \dots, \\ h_1^\pm &= c_\eta^{h_1^\pm} \rho^{|n\mp m|} + \dots, & h_2^\pm &= c_\eta^{h_2^\pm} \rho^{|n-\nu\mp m|} + \dots, \end{aligned} \quad (3.32)$$

where $c_\eta^Z, c_\eta^A, c_\eta^{W^\pm}, c_\eta^{h_a^\pm}$ are 16 integration constants and the dots stand for subleading terms.

We are interested in bound state type solutions for which $\Psi \rightarrow 0$ as $\rho \rightarrow \infty$. In order to work out their behavior at large ρ , it is convenient to temporarily pass to the gauge where $f_2(\infty) = 0$. This is achieved by applying the global symmetry (2.10) with $\Gamma = -\gamma$, which corresponds to the gauge transformation (2.2) with $U = \exp\{\frac{i}{2}\gamma\}$. The background fields then simplify and one finds at large ρ

$$\begin{aligned} \mathcal{Z}_\eta &= \frac{b_\eta^Z}{\sqrt{\rho}} e^{-\mu_Z \rho} + \dots, & \mathcal{A}_\eta &= \frac{b_\eta^A}{\sqrt{\rho}} e^{-\mu_A \rho} + \dots, & h_1^+ + h_1^- &= \frac{b_+^{h_1}}{\sqrt{\rho}} e^{-\mu_Z \rho} + \dots, \\ \mathcal{W}_\eta^\pm &= \frac{b_\eta^{W^\pm}}{\sqrt{\rho}} e^{-\int \mu_{W^\pm} d\rho} + \dots, & h_2^\pm &= \frac{b_\pm^{h_2}}{\sqrt{\rho}} e^{-\int \mu_{W^\pm} d\rho} + \dots, & h_1^+ - h_1^- &= \frac{b_-^{h_1}}{\sqrt{\rho}} e^{-\mu_H \rho} + \dots \end{aligned} \quad (3.33)$$

Here the effective mass terms

$$\mu_A^2 = \kappa^2 - \omega^2, \quad \mu_Z^2 = \mu_A^2 + m_Z^2, \quad \mu_H^2 = \mu_A^2 + m_H^2, \quad \mu_{W^\pm}^2(\rho) = (\sigma u(\rho) \pm \kappa)^2 - \omega^2 + m_W^2 \quad (3.34)$$

are assumed to be positive and $b_\eta^Z, b_\eta^A, b_\eta^{W^\pm}, b_\eta^{h^\pm}$ are 16 integration constants while the dots stand for the subleading terms. One can now apply to the whole system (background + perturbations) the inverse gauge rotation with $U = \exp\{-\frac{i}{2}\gamma\}$. The background then returns to the gauge where $f_2(\infty) = \sin \frac{\gamma}{2}$ while the perturbations (3.33) change as

$$\begin{aligned}
\mathcal{Z}_\eta &\rightarrow (g'^2 + g^2 \cos \gamma) \mathcal{Z}_\eta + 2gg' \sin^2 \frac{\gamma}{2} \mathcal{A}_\eta - \frac{g}{\sqrt{2}} \mathcal{W}_\eta^+ \sin \gamma - \frac{g}{\sqrt{2}} \mathcal{W}_\eta^- \sin \gamma, \\
\mathcal{A}_\eta &\rightarrow (g^2 + g'^2 \cos \gamma) \mathcal{A}_\eta + 2gg' \sin^2 \frac{\gamma}{2} \mathcal{Z}_\eta + \frac{g'}{\sqrt{2}} \mathcal{W}_\eta^+ \sin \gamma + \frac{g'}{\sqrt{2}} \mathcal{W}_\eta^- \sin \gamma, \\
\mathcal{W}_\eta^+ &\rightarrow \mathcal{W}_\eta^+ \cos^2 \frac{\gamma}{2} - \mathcal{W}_\eta^- \sin^2 \frac{\gamma}{2} + \frac{g}{\sqrt{2}} \mathcal{Z}_\eta \sin \gamma - \frac{g'}{\sqrt{2}} \mathcal{A}_\eta \sin \gamma, \\
\mathcal{W}_\eta^- &\rightarrow \mathcal{W}_\eta^- \cos^2 \frac{\gamma}{2} - \mathcal{W}_\eta^+ \sin^2 \frac{\gamma}{2} + \frac{g}{\sqrt{2}} \mathcal{Z}_\eta \sin \gamma - \frac{g'}{\sqrt{2}} \mathcal{A}_\eta \sin \gamma, \\
h_1^\pm &\rightarrow h_1^\pm \cos \frac{\gamma}{2} - h_2^\pm \sin \frac{\gamma}{2}, \quad h_2^\pm \rightarrow h_2^\pm \cos \frac{\gamma}{2} + h_1^\pm \sin \frac{\gamma}{2}.
\end{aligned} \tag{3.35}$$

This gives the large ρ behavior of perturbations. At this point we have everything we need to solve the perturbation equations (3.30).

IV. STABILITY TEST

Summarizing the above analysis, we have arrived at the eigenvalue problem (3.30) and now we wish to know whether it admits bound state solutions with $\omega^2 < 0$. If exist, such solutions would correspond to unstable modes of the background vortex. In order to detect them, one possibility is to directly integrate the 16 coupled second order differential equations (3.30). However, if one just wants to know if negative modes exist or not, it is not necessary to construct them explicitly. A simple method to reveal their existence is to use the Jacobi criterion [20], which essentially uses the fact that the ground state wave function does not oscillate while the excited states do. It follows that if the zero energy wave function oscillates then the ground state energy is negative.

A. Jacobi criterion

When applied to our problem the Jacobi method gives the following recipe. Let $\Psi_s(\rho)$ with $s = 1, \dots, 16$ be the 16 linearly independent, regular at the symmetry axis solutions of (3.30). Each of them is a 16-component vector, $\Psi_s(\rho) \equiv \Psi_s^I(\rho)$, $I = 1, \dots, 16$. Let $\Delta(\rho)$ be

the determinant of the matrix $\Psi_s^I(\rho)$. If it vanishes somewhere, then there exists a negative part of the spectrum. According to [21], the number of zeros of $\Delta(\rho)$ is equal to the number of negative modes.

Calculating $\Delta(\rho)$ is a much easier task than solving the boundary value problem (3.30), since this simply requires to integrate the equations starting from $\rho = 0$ with the boundary conditions (3.32). This should be done, in principle, for each pair of values κ, m . In [16] this method was used to test stability in the semilocal limit, where $\theta_w = \pi/2$, while the typical behavior of the Jacobi determinant $\Delta(\rho)$ for $\theta_w < \pi/2$ is shown in Figs.2,3.

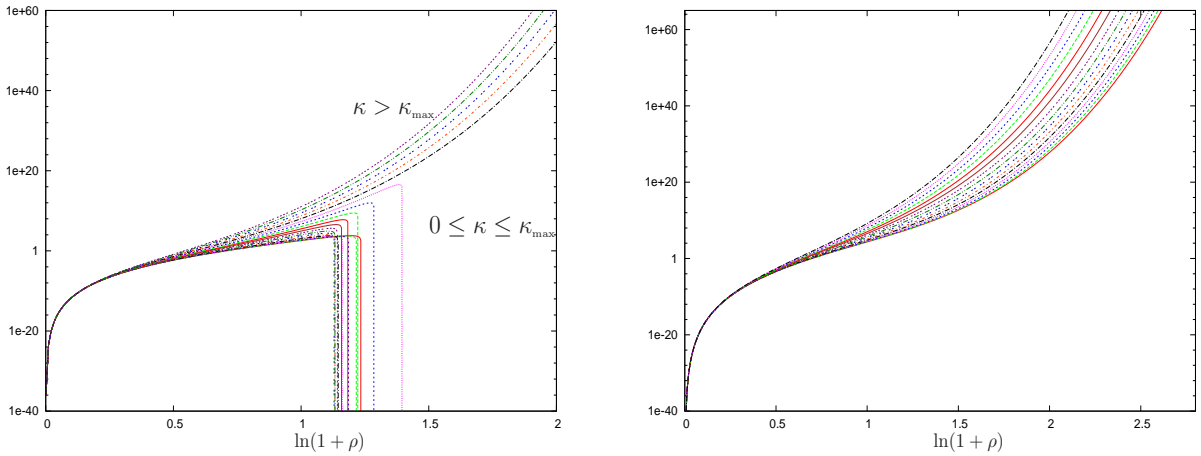


Figure 2: The behavior of the Jacobi determinant $\Delta(\rho)$ for fluctuations around the $n = \nu = 1$, $\mathcal{I} = 0.87$ vortex ($\beta = 2$, $\sin^2 \theta_w = 0.23$) for different values of κ for $m = 0$ (left) and for $m = 1$ (right). The behavior for $m = 2$ is qualitatively the same as for $m = 1$.

The main observation is as follows: the fundamental vortex with $n = \nu = 1$ has one negative mode in the $m = 0$ sector for every value of κ from the interval

$$|\kappa| < \kappa_{\max}(\mathcal{I}). \quad (4.36)$$

This can be seen in Fig.2 where $\Delta(\rho)$ passes through zero exactly once if κ is small and never vanishes if κ is large. In fact, the symmetry relations (3.31) imply that $\omega^2(-\kappa, -m) = \omega^2(\kappa, m)$, so that for $m = 0$ one has $\omega^2(-\kappa) = \omega^2(\kappa)$ and it is therefore sufficient to consider only the $\kappa \geq 0$ region. In the Z string limit, for $\mathcal{I} = 0$, one finds

$$\kappa_{\max}(0) = 2\sigma(0) \quad (4.37)$$

(see Table I) and also $\omega^2(0) = 0$, so that the $\kappa = 0$ mode is not negative. For $\mathcal{I} \neq 0$ one has

$$\kappa_{\max}(\mathcal{I}) > 2\sigma(\mathcal{I}), \quad (4.38)$$

and in addition we find that the $\kappa = 0$ mode is negative for $\theta_w \neq \pi/2$,

$$\omega^2(0) < 0, \quad \mathcal{I} \neq 0, \quad (4.39)$$

while in the semilocal limit one has $\omega^2(0) = 0$ for all values of \mathcal{I} [16].

It seems that for the $n = \nu = 1$ vortex there are no other instabilities. We have checked for different values of κ that for $m = 1, 2$ there are no negative modes (see Fig.2), while further increasing m increases the centrifugal energy thus rendering the existence of bound states less probable. As a result, it seems that the $n = \nu = 1$ vortices are unstable only in the $m = 0$ sector and are stable with respect to any other perturbations.

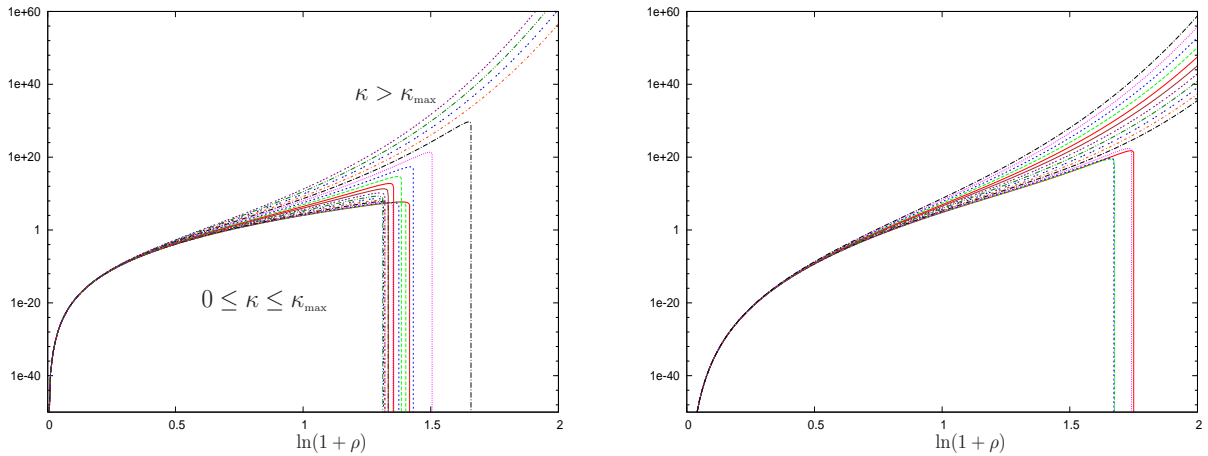


Figure 3: The Jacobi determinant for fluctuations around the $n = \nu = 2$ vortex with $\mathcal{I} = 0.87$ ($\beta = 2$, $\sin^2 \theta_w = 0.23$) in the $m = 0$ (left) and $m = 2$ (right) sectors for different values of κ .

We also considered vortices with higher winding numbers n and ν and found that the axially symmetric sector remains unstable for all solutions we examined (this was checked up to $n = 3$). An example is shown in Fig.3 for $n = \nu = 2$. This instability is qualitatively the same as for the $n = \nu = 1$ vortex, it exists for $0 < |\kappa| < \kappa_{\max}(\mathcal{I})$. However, solutions with $n > 1$ have additional instabilities in sectors with $m > 1$ which can be interpreted as splitting modes. For example, the $n = 2$ solutions are also unstable in the $m = 2$ sector (see Fig.3), which apparently corresponds to breaking of the $n = 2$ vortex into two $n = 1$ vortices. Such splitting instabilities are less interesting for us, and in what follows we shall concentrate on the intrinsic instability of the fundamental $n = 1$ vortex.

B. Finding the eigenvalue

Having detected the negative modes, we now wish to construct them explicitly. Such a construction is considerably more involved than applying the Jacobi criterion, since it requires to solve the boundary value problem for the 16 coupled equations (3.30) with the boundary conditions (3.32) and (3.35). Unfortunately, even for $m = 0$ these equations do not simplify much. We solve them with the multiple shooting method [22], which requires to match at a fitting point the values of the 16 functions and their 16 first derivatives. It is then important to have enough free parameters in our disposal, and in fact we have the 16 integration constants in the local solutions (3.32), then 16 other constants in (3.35), and also the eigenvalue ω^2 . As we consider a linear system, one constant can be fixed by the overall renormalization, so that there remain 32 parameters to fulfill the 32 matchings conditions. Resolving these conditions gives us the global solution $\Psi(\rho)$ of Eqs.(3.30) in the interval $\rho \in [0, \infty)$ and also the eigenvalue ω^2 .

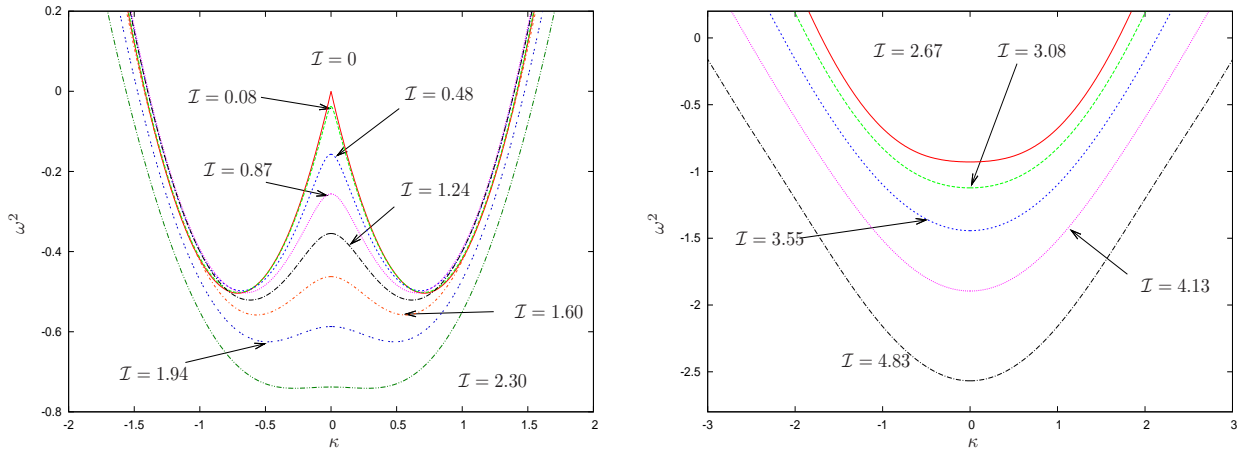


Figure 4: Dispersion relation $\omega^2(\kappa)$ for the $m = 0$ bound state solutions of Eqs.(3.30) for the $n = \nu = 1$ vortex ($\beta = 2$, $\sin^2 \theta_w = 0.23$) for $\mathcal{I} < \mathcal{I}_* = 2.57$ (left) and for $\mathcal{I} > \mathcal{I}_*$ (right).

As a result, we obtain the dispersion relation $\omega^2(\kappa)$ shown in Fig.4. We see that there is a value $\kappa_{\max}(\mathcal{I})$ such that $\omega^2(\kappa) < 0$ for $|\kappa| < \kappa_{\max}$. For small currents the function $\omega^2(\kappa)$ has a double-well shape, with two minima of equal depth at $\kappa = \pm\kappa_{\min}$ and a local negative maximum at $\kappa = 0$. As the current increases, κ_{\min} decreases, the value $\omega^2(0)$ approaches $\omega^2(\pm\kappa_{\min})$, and finally κ_{\min} vanishes for $\mathcal{I} = \mathcal{I}_*$ when all three extrema of $\omega^2(\kappa)$ merge into a global minimum. For $\mathcal{I} > \mathcal{I}_*$ the function $\omega^2(\kappa)$ shows only one global minimum at $\kappa = 0$.

Some numerical characteristics of $\omega^2(\kappa)$ are presented in Table I.

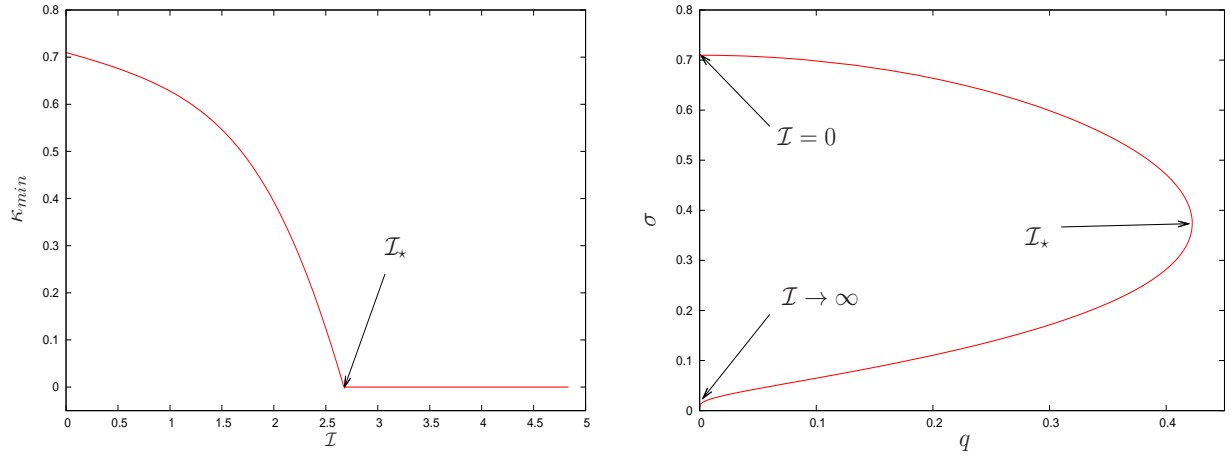


Figure 5: Profiles of $\kappa_{\max}(\mathcal{I})$ (left) and $\sigma(\mathcal{I})$ against $q(\mathcal{I})$ (right) for the same vortex solution as in Fig.4.

The passage from the two-well to one-well structure of the dispersion relation suggests that the system undergoes some kind of phase transition at $\mathcal{I} = \mathcal{I}_*$. This is corroborated by the profile of $\kappa_{\min}(\mathcal{I})$ (see Fig.5) reminding of a second order phase transition. The point $\mathcal{I} = \mathcal{I}_*$ is also distinguished by the fact that the background ‘consensate parameter’ $q = f_2(0)$ attains its maximal value there (see Fig.5). When \mathcal{I} grows further, q starts decreasing and tends to zero as $\mathcal{I} \rightarrow \infty$. For large currents the vortex shows in its central part an unbroken phase region where the Higgs field is driven to zero by the strong magnetic field [12]. This suggest that the point $\mathcal{I} = \mathcal{I}_*$ corresponds to the transition in which the unbroken phase just starts to appear in the vortex center. The plot $\sigma(q)$ shows a characteristic two-branch structure (see Fig.5) and the point $\mathcal{I} = \mathcal{I}_*$ corresponds to the bifurcation between the two branches. Although this suggest that the stability may change at this point, we know already that the number of instabilities remains actually the same, but the dispersion relation changes its shape. As discussed in Sec.VII below, this should alter the generic instability pattern.

Let us now consider the limiting cases where the vortex current is either small or large. This will help to understand the structure of curves in Fig.4.

Table I: Parameter values for the $n = \nu = 1$ vortices with $\beta = 2$, $\sin^2 \theta_{\text{W}} = 0.23$.

\mathcal{I}	σ	$\omega^2(0)$	κ_{\min}	$\omega^2(\kappa_{\min})$	κ_{\max}
0	0.709697	0.0	0.709697	-0.503670	1.419394
0.0804	0.700	-0.0370976	0.705	-0.519740	1.415
0.4851	0.650	-0.157024	0.680	-0.497821	1.395
0.8739	0.600	-0.255942	0.655	-0.502902	1.390
1.2430	0.550	-0.354806	0.615	-0.520995	1.400
1.6002	0.500	-0.462475	0.570	-0.558202	1.425
1.9494	0.450	-0.587058	0.475	-0.625174	1.475
2.3004	0.400	-0.738065	0.280	-0.741152	1.560
2.6740	0.350	-0.928761	0.0	-0.928761	1.695
3.0831	0.300	-1.12311	0.0	-1.12311.	1.855
3.5594	0.250	-1.44332	0.0	-1.44332.	2.135
4.1327	0.200	-1.89531	0.0	-1.89531.	2.550
4.8335	0.150	-2.56766	0.0	-2.56766.	3.150

V. ZERO CURRENT LIMIT

When the vortex current tends to zero, the solutions reduce to Z strings [7], whose stability has been studied before [13], [14]. The most detailed consideration of the problem was presented in Ref.[13], whose results we have been able to confirm.

In zero current limit the vortex field amplitudes become

$$\begin{aligned}
 u &= -1, & v &= 2g^2(v_{\text{ANO}} - n) + 2n - \nu \equiv v_{\text{Z}}, & u_1 &= 0, & u_3 &= 1, \\
 v_1 &= 0, & v_3 &= 2g^2(v_{\text{ANO}} - n) + \nu \equiv v_{\text{Z3}}, & f_1 &= f_{\text{ANO}} \equiv f_{\text{Z}}, & f_2 &= 0,
 \end{aligned}
 \tag{5.40}$$

and the field equations (A.1)–(A.9) reduce to the ANO system

$$\begin{aligned}
 \frac{1}{\rho}(\rho f'_{\text{ANO}})' &= \left(\frac{v_{\text{ANO}}^2}{\rho^2} + \frac{\beta}{4}(f_{\text{ANO}}^2 - 1) \right) f_{\text{ANO}}, \\
 \rho \left(\frac{v'_{\text{ANO}}}{\rho} \right)' &= \frac{1}{2} f_{\text{ANO}}^2 v_{\text{ANO}}
 \end{aligned}
 \tag{5.41}$$

whose solutions fulfill the boundary conditions $0 \leftarrow f_{\text{ANO}} \rightarrow 1$ and $n \leftarrow v_{\text{ANO}} \rightarrow 0$ as $0 \leftarrow \rho \rightarrow \infty$. The solutions depend only on the winding number n , although when written in the gauge (2.9) the fields also contain σ_α, ν ,

$$\mathcal{W}_Z = (\tau^3 - 1) \sigma_\alpha dx^\alpha - [v_Z(\rho) + \tau^3 v_{Z3}(\rho)] d\varphi, \quad \Phi_Z = \begin{pmatrix} f_Z(\rho) \\ 0 \end{pmatrix}. \quad (5.42)$$

The values of σ^2, ν are determined by those for the generic vortices in the $\mathcal{I} \rightarrow 0$ limit, one has for example $\sigma^2 = \sigma^2(\beta, \theta_w, n, \nu) > 0$. Although σ_α, ν can be gauged away for this solution, they reappear again in the perturbation equations. In particular, $-\sigma^2$ determines (see (5.46)) the eigenvalue in Eqs.(5.43), and since it is negative, Z strings are unstable. Stable Z strings also exist, for unphysical values of β, θ_w (the eigenvalue is then positive), but they cannot be viewed as limits of superconducting vortices [12], so that they are not relevant for us. One can accurately determine the parameter regions in the β, θ_w plane where Z strings are unstable/stable and so can/cannot be promoted to the superconducting vortices by studying solutions of Eqs.(5.43) with $\sigma^2 = 0$ [13], [12].

Imposing (5.40), the potential energy matrix in the Schrödinger operator (B.1) becomes block diagonal, so that the space of perturbations spanned by the 16-component vector Ψ in (B.2) decomposes into a direct sum of six one-dimensional subspaces, one four-dimensional subspace, and two three-dimensional subspaces. The six one-dimensional subspaces are spanned by $\mathcal{A}_{\pm 1}, \mathcal{A}_0, \mathcal{Z}_0, \mathcal{W}_0^\pm$, which describe the photon and the longitudinal components of Z and W bosons. The potentials in the corresponding one-channel Schrödinger equations are positive definite so that there are no negative modes in these sectors.

The four-dimensional subspace is spanned by \mathcal{Z}_\pm, h_1^\pm , which correspond to the transverse components of Z and Higgs bosons. For $m = 0$ this space further splits into sectors spanned, respectively, by $\mathcal{Z}_+ + \mathcal{Z}_-, h_1^+ + h_1^-$ and by $\mathcal{Z}_+ - \mathcal{Z}_-, h_1^+ - h_1^-$. Both of them contain bound states with $\omega^2 > 0$ (in the first sector they exist only for $\beta < 1.5$) but there are no negative modes in this case.

The remaining three-dimensional subspaces spanned by \mathcal{W}_+^\pm, h_2^+ and \mathcal{W}_-^\pm, h_2^- contain the negative modes. The perturbations are governed in this case by

$$-\frac{1}{\rho} (\rho \Psi'_\pm)' + \mathcal{U}_\pm \Psi_\pm = \Lambda_\pm \Psi_\pm \quad (5.43)$$

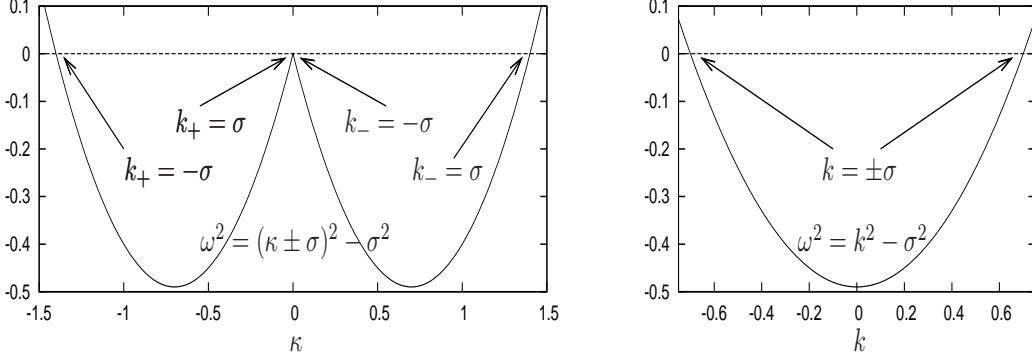


Figure 6: Dispersion relation (5.47) for the bound state solutions of the eigenvalue problem (5.43) (left). The two parabolas correspond to solutions in the independent Ψ_+ and Ψ_- sectors. Passing to the gauge (5.48) they get mapped into one parabola giving the dispersion relation for the modes (5.49) (right). The arrows indicate bifurcations with the superconducting branch.

with $\Lambda_{\pm} = \omega^2 - (\sigma \mp \kappa)^2$ and

$$\Psi_{\pm} = \begin{pmatrix} \mathcal{W}_+^{\pm} \\ \mathcal{W}_-^{\pm} \\ h_2^{\pm} \end{pmatrix}, \quad \mathcal{U}_{\pm} = \begin{pmatrix} \Delta_{+1}^{\mathcal{W}^{\pm}} & 0 & V^{\pm} \\ 0 & \Delta_{-1}^{\mathcal{W}^{\pm}} & V^{\mp} \\ V^{\pm} & V^{\mp} & \Delta_{\pm}^{h_2} \end{pmatrix}, \quad (5.44)$$

where

$$\begin{aligned} \Delta_{\eta}^{\mathcal{W}^{\pm}} &= \frac{(2g^2(v_{\text{ANO}} - n) + \nu \pm (m - \nu))^2}{\rho^2} \pm 4\eta g^2 \frac{v'_{\text{ANO}}}{\rho} + \frac{g^2}{2} f_{\text{ANO}}, \\ \Delta_{\pm}^{h_2} &= \frac{(v_{\text{ANO}} \mp m)^2}{\rho^2} + \frac{\beta}{4} (f_{\text{ANO}}^2 - 1) + \frac{g^2}{2} f_{\text{ANO}}, \quad V^{\pm} = g \left(f'_{\text{ANO}} \pm \frac{v_{\text{ANO}} f_{\text{ANO}}}{\rho} \right). \end{aligned} \quad (5.45)$$

For $m = 0$ equations (5.43) admit bound state solutions both in the Ψ_+ and Ψ_- subspaces with the eigenvalue

$$\Lambda_+ = \Lambda_- = -\sigma^2 \equiv -\sigma^2(\beta, \theta_w, n, \nu) < 0 \quad (5.46)$$

for $\nu = 1, \dots, \nu_{\text{max}}$ where $n \leq \nu_{\text{max}}(\beta, \theta_w, n) \leq 2n - 1$ [12]. These bound states are characterized, respectively, by the dispersion relation

$$\omega^2 = \omega_{\pm}^2(\kappa) \equiv (\sigma \mp \kappa)^2 - \sigma^2 = \kappa(\kappa \mp 2\sigma). \quad (5.47)$$

One has $\omega_+^2(\kappa) < 0$ for $0 < \kappa < 2\sigma$ and $\omega_-^2(\kappa) < 0$ for $-2\sigma < \kappa < 0$ so that there is one negative mode for every value of κ from the interval $(-2\sigma, 0) \cup (0, 2\sigma)$. As a result, the dispersion relation for negative modes is described by $\omega_+^2(\kappa)$ for $\kappa > 0$ and by $\omega_-^2(\kappa)$

for $\kappa < 0$, therefore the $\omega^2(\kappa)$ curve consists of two parabolas intersecting at $\kappa = 0$ (see Fig.6). These parabolas continue to the $|\kappa| > 2\sigma$ regions where there are bound states with $\omega^2 > 0$. However, they should terminate for $\kappa = 0$, since the effective photon mass $\mu_A^2 = \kappa^2 - \omega^2 = \pm 2\sigma\kappa$ defined by Eq.(3.34) becomes imaginary after this point. Although the photon decouples for exactly vanishing background current, it rests coupled for however small but non-zero currents, when the background is arbitrarily close to Z string.

Let us now use (3.19) to reconstruct the dependence of negative modes on all spacetime coordinates. Then we apply to (5.42) the gauge transformation $U = e^{in\varphi}u(\nu\varphi)u(\sigma_\alpha x^\alpha)$ with $u(X) \equiv e^{iX(1-\tau^3)/2}$. The Z string becomes then globally regular and independent of σ_α, ν ,

$$\mathcal{W}_Z^{\text{reg}} = 2(g'^2 + g^2\tau^3)(n - v_{\text{ANO}}(\rho))d\varphi, \quad \Phi_Z^{\text{reg}} = \begin{pmatrix} e^{in\varphi}f_{\text{ANO}}(\rho) \\ 0 \end{pmatrix}, \quad (5.48)$$

in which form it is usually described in the literature [7]. The negative modes read in this gauge (writing down only the Higgs field perturbations) $\delta\Phi_2 = C_+h_2^+(\rho)e^{|\omega_+(k_+)|t}e^{-ik_+z}$ for $\kappa \in (0, 2\sigma)$ and $\delta\Phi_2 = C_-h_2^-(\rho)e^{|\omega_-(k_-)|t}e^{ik_-z}$ for $\kappa \in (-2\sigma, 0)$. Here C_\pm are integration constants, $k_\pm = \kappa \mp \sigma$ and $\omega_\pm^2 = k_\pm^2 - \sigma^2$. Replacing $k_\pm \rightarrow k$ and using the fact that $h_2^+(\rho) = h_2^-(\rho)$ one can write these solutions simply as

$$\delta\Phi_2 = C_\pm h_2^\pm(\rho)e^{|\omega(k)|t}e^{\mp ikz} \quad (5.49)$$

with $\omega^2 = k^2 - \sigma^2$ (see Fig.6). These negative modes can be viewed as standing waves of length $\lambda = 2\pi/k$ whose amplitude grows in time. For $k = \pm\sigma$ one obtains zero modes corresponding to the bifurcations of Z strings with the superconducting solutions. Since the minimal wavelength of negative modes is $\lambda_{\text{min}} = 2\pi/\sigma$, this suggests that the instability could be removed by imposing periodic boundary conditions along the z -axis with the period $L \leq \lambda_{\text{min}}$. However, this would not remove the homogeneous $k = 0$ mode, $\delta\Phi_2 = Ch_2^+(\rho)e^{\sigma t}$, since it is independent of z and so can be considered as periodic with any period.

Let us, however, consider Z string in yet another gauge – the one given by Eq.(2.12). In this gauge the fields are also globally regular (we assume the restframe condition $\sigma_\alpha = \sigma\delta_\alpha^3$),

$$\mathcal{W} = \sigma(\tau^3 - 1)dz + \mathcal{W}_Z^{\text{reg}}, \quad \Phi = \Phi_Z^{\text{reg}}. \quad (5.50)$$

The correspondence between this gauge and (5.48) is provided by the gauge transformation with

$$U = u(\sigma z) = \begin{bmatrix} 1 & 0 \\ 0 & e^{i\sigma z} \end{bmatrix}. \quad (5.51)$$

The negative modes (5.49) now become

$$\delta\Phi_2 = C_{\pm} h_2^+(\rho) e^{|\omega_{\pm}(\kappa)|t} e^{\mp i\kappa z} \quad (5.52)$$

with $\kappa \in (-2\sigma, 0) \cup (0, 2\sigma)$, these are standing waves of length $\lambda = 2\pi/\kappa \geq \lambda_{\min} = \pi/\sigma$. Imposing now periodic boundary conditions with period $L = \pi/\sigma$ will remove *all* negative modes. In particular, the mode which used to be homogeneous becomes now z -dependent with $\kappa = \pm\sigma$, so that it will be removed. The z -independent mode now corresponds to $\kappa = 0$ and it will not be removed, but this mode is *not negative*, so it is harmless. One should say that in the case under consideration all gauge invariant quantities like $\delta B_{\mu\nu}$ and $\delta(n^a W_{\mu\nu}^a)$ vanish and there is no gauge invariant way to decide which modes are homogeneous.

We notice finally that the gauge transformation (5.51) is *not* periodic in the interval $[0, \pi/\sigma]$, and therefore imposing the periodicity breaks the gauge equivalence between (5.48) and (5.50). The two descriptions of Z string become therefore physically different, which is why (5.50) becomes stable upon imposing the periodicity while (5.48) rests unstable. To the best of our knowledge, such a possibility to stabilize Z strings has never been discussed in the literature.

Since the Z string zero modes for $\kappa = \pm 2\sigma$ correspond to bifurcations with the superconducting solutions, they can be viewed as small deformations induced by the current. Now, one has $\omega^2(\pm\kappa_{\max}) = 0$ also for $\mathcal{I} \neq 0$, which suggests that the related zero modes also correspond to deformations induced by a small current variation. However, for $\mathcal{I} \neq 0$ such deformations would inevitably contain logarithmically growing at infinity terms and therefore would not correspond to bound state solutions of the perturbation equations. This suggests that the $\kappa = \pm\kappa_{\max}$ zero modes could correspond to variations with respect to some other parameter. In other words, it may be that the vortex solutions admit stationary generalizations within a field ansatz more general than (2.9).

VI. LARGE CURRENT LIMIT

When the current \mathcal{I} is large, the vortex develops in its center a region of size $\sim \mathcal{I}$ where the magnetic field is so strong that it quenches the Higgs field to zero. Most of this region is filled with the massless electromagnetic and Z fields produced by the current. The latter is carried by the charged W boson condensate confined in the compact core of size $\sim 1/\mathcal{I}$ placed

in the very center of the symmetric phase. Outside the symmetric phase region the Higgs field relaxes to its vacuum value and everything reduces to the ordinary electromagnetic Biot-Savart field [12].

The vortex fields in this limit can be described by splitting the space into two parts: the core region $\rho < x_0/\mathcal{I}$ and the exterior region $\rho > x_0/\mathcal{I}$. The fields in the core can be approximated by

$$\begin{aligned} f_1 = f_2 = \sigma u_3 = v_1 = 0, \quad \sigma u = \text{const.}, \quad v = 1, \\ \sigma u_1(\rho) = \mathcal{I}U_1(\mathcal{I}\rho), \quad v_3 = V_3(\mathcal{I}\rho), \end{aligned} \quad (6.53)$$

in which case the field equations (A.1)–(A.9) reduce to

$$\frac{1}{x}(xU_1')' = \frac{V_3^2}{x^2}U_1, \quad x\left(\frac{V_3'}{x}\right)' = U_1^2V_3, \quad (6.54)$$

with $x = \mathcal{I}\rho$. The solution of these equations exhibits the following behavior for $0 \leftarrow x \rightarrow \infty$,

$$0 \leftarrow U_1(x) \rightarrow a \ln x + b, \quad 1 \leftarrow V_3(x) \rightarrow 0 \quad (6.55)$$

(here $a = 0.29, b = -0.08$ if $g^2 = 0.23$) where the large x asymptotic is attained, up to exponentially small terms, at $x \equiv x_0 \approx 10$. This determines the size of the core region. This solution describes the current-carrying charged W condensate confined in the core, the current value entering (6.53) as the scale parameter.

The fields for $\rho > x_0/\mathcal{I}$ can be found separately and then matched to the core fields at $\rho = x_0/\mathcal{I}$ [12]. We do not need here the precise form of the $\rho > x_0/\mathcal{I}$ solutions, since it is sufficient to analyze the stability of the core region. Indeed, suppose that we find a negative mode localized in the core. Since it vanishes in the outside region, it fulfills the perturbation equations also there, so that it will be a negative mode of the whole vortex configuration. In principle there could be additional negative modes in the outside region, however, it turns out that the core negative modes fit in well with the general instability pattern described above, which suggests that all vortex instabilities are localized in its core.

To study the core instabilities, we inject (6.53) into the perturbation equations (B.1). Passing to the radial variable $x = \mathcal{I}\rho$ and defining

$$\tilde{\omega} = \omega/\mathcal{I}, \quad \tilde{\kappa} = \kappa/\mathcal{I}, \quad (6.56)$$

the current \mathcal{I} drops from the equations. For $m = 0$ the equations split into three independent multichannel sectors plus free wave equations, and applying the Jacobi criterion one can check that the negative modes are contained only in the sector spanned by five amplitudes

$$\begin{aligned} Y_4^2 &\equiv X_1(x), & Y_2^3 &\equiv X_2(x), & X_4^3 &\equiv X_5(x), \\ \sqrt{2} X_3^1 &\equiv x (X_3(x) - X_4(x)), & \sqrt{2} X_2^2 &\equiv X_3(x) + X_4(x). \end{aligned} \quad (6.57)$$

Introducing the five-component vector and the potential energy matrix

$$\Psi = \begin{pmatrix} X_1 \\ X_2 \\ X_3 \\ X_4 \\ X_5 \end{pmatrix}, \quad \mathcal{U} = \begin{pmatrix} M_1 & Q & 0 & 0 & R \\ Q & M_2 & S & S & 0 \\ 0 & S & M_+ & T & U_+ \\ 0 & S & T & M_- & U_- \\ R & 0 & U_+ & U_- & M_0 \end{pmatrix} \quad (6.58)$$

with the matrix elements

$$\begin{aligned} M_1 &= \frac{V_3^2}{x^2} + U_1^2, & M_2 &= \frac{1}{x^2} + U_1^2, & M_{\pm} &= \frac{(V_3 \mp 1)^2}{x^2} \pm \frac{2\partial_x V_3}{x} + U_1^2, & M_0 &= U_1^2, \\ Q &= -\sqrt{2}\partial_x U_1, & R &= -\sqrt{2}S = -2\tilde{\kappa}U_1, & U_{\pm} &= \sqrt{2} \left(\partial_x U_1 \pm \frac{U_1 V_3}{x} \right), & T &= \frac{U_1^2}{2}, \end{aligned} \quad (6.59)$$

the unstable sector is described by

$$-\frac{1}{x} (x\Psi'_x)' + \mathcal{U}\Psi = \Lambda\Psi, \quad (6.60)$$

where $\Lambda = \tilde{\omega}^2 - \tilde{\kappa}^2$. Fig.7 shows the Jacobi determinant $\Delta(\rho)$ for various values of $\tilde{\kappa}$, and it seems that it always has a zero at some ρ , at least we could not find an upper bound $\tilde{\kappa}_{\max}$ beyond which $\Delta(\rho)$ ceases to vanish. Since such a bound always exists for small currents, it should presumably exist also for large currents, but to find it one should probably refine the approximation (6.60) to take into account the region outside the core. At present, it seems that the description (6.60) is valid for any $\tilde{\kappa}$ if $\mathcal{I} \rightarrow \infty$ or, if \mathcal{I} is large but finite, up to some large but finite value of $\tilde{\kappa}$.

We then solve the eigenvalue problem (6.60) looking for bound states with the boundary conditions $X_3 \sim X_5 = O(1)$, $X_1 \sim X_2 = O(x)$, $X_4 = O(x^2)$ at small x , while at large x

$$\begin{aligned} X_1 \pm X_5 &\sim X_3 + X_4 \mp \sqrt{2}X_2 \sim \exp\left\{-\int^x \sqrt{(U_1 \mp \tilde{\kappa})^2 - \tilde{\omega}^2} dx\right\}, \\ X_3 - X_4 &\sim \exp\{-\sqrt{\tilde{\kappa}^2 - \tilde{\omega}^2} x\}. \end{aligned} \quad (6.61)$$

This gives the dispersion relation $\tilde{\omega}^2(\tilde{\kappa})$ shown in Fig.7, from where

$$\omega^2(\kappa) = \mathcal{I}^2 \tilde{\omega}^2(\kappa/\mathcal{I}). \quad (6.62)$$

We see that the negative mode eigenvalue is large for large currents, $\omega \sim \mathcal{I}$, which relates

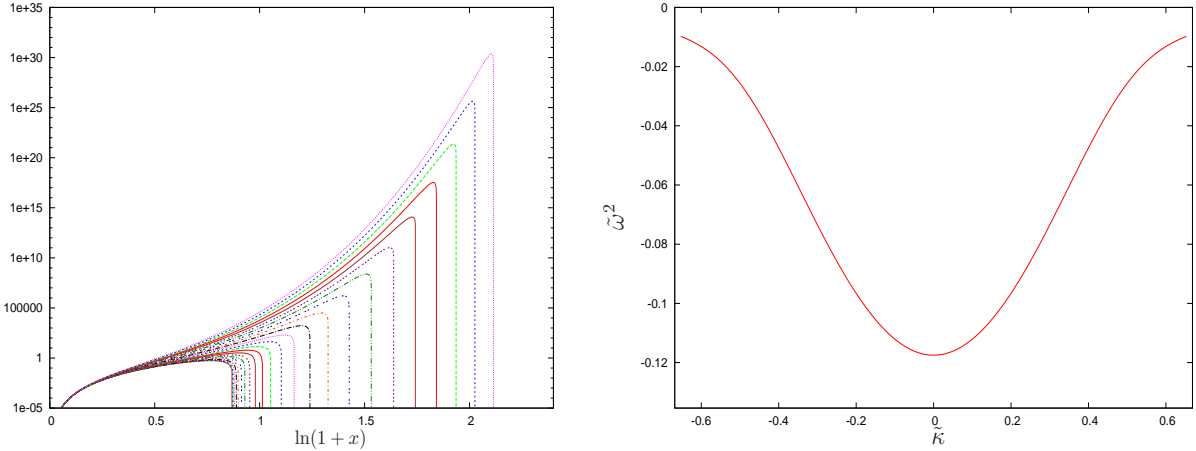


Figure 7: The Jacobi determinant for Eqs.(6.60) for various values of $\tilde{\kappa}$ (left) and the dispersion relation $\tilde{\omega}^2(\tilde{\kappa})$ (right) for the $n = \nu = 1$, $\beta = 2$, $\sin^2 \theta_w = 0.23$ vortex in the large current limit.

to the fact that the corresponding eigenmode is localized within a very short interval of size $\sim 1/\mathcal{I}$ inside the core. It is worth noting that the one-well shape of this dispersion relation is qualitatively similar to what is shown in Fig.4. This suggests that the approximate description provided by Eqs.(6.60) is essentially correct. Since the ratio κ/\mathcal{I} is small unless κ is very large, one has

$$\omega^2(\kappa) \approx \mathcal{I}^2 \tilde{\omega}^2(0) \approx -0.12 \mathcal{I}^2, \quad (6.63)$$

where the numerical coefficient is calculated for $n = \nu = 1$, $\beta = 2$, $\sin^2 \theta_w = 0.23$.

VII. CHARGED VORTICES

Let us consider a bound state solution $\Psi_\kappa(\rho)$ of the Schrödinger problem (3.30) with the eigenvalue $\omega^2(\kappa)$ (setting for simplicity $m = 0$). Injecting it into the mode decomposition (3.19) we reconstruct the dependence on all spacetime variables. The result will be a superposition of the real and imaginary parts of

$$e^{i\Xi(t,z)} \Psi_\kappa(\rho). \quad (7.64)$$

Here, using (2.8),

$$\Xi(t, z) = \omega_b t + \kappa_b z \quad (7.65)$$

with (ω_b, κ_b) being the Lorentz-transformed (boosted) components of the spacetime vector (ω, κ) ,

$$\omega_b = \cosh(b) \omega + \sinh(b) \kappa, \quad \kappa_b = \cosh(b) \kappa + \sinh(b) \omega. \quad (7.66)$$

The boost parameter is related to the electric charge $I_0 = \mathcal{I} \sinh(b)$ (see (2.13)). Suppose that the mode under consideration is negative, $\omega^2 < 0$, so that $\omega = i|\omega|$. Then

$$\exp(i\Xi) = \exp\{|\omega|(\cosh(b)t + \sinh(b)z)\} \exp\{i\kappa(\sinh(b)t + \cosh(b)z)\}. \quad (7.67)$$

Let us consider first the uncharged vortex, for which one has $b = I_0 = 0$ and so

$$\exp(i\Xi) = \exp(|\omega|t) \exp(i\kappa z), \quad (7.68)$$

which grows in time but is periodic along z . Let us call such negative modes ‘proper’. The effect of this instability is schematically shown in Fig.8 – the vortex undergoes inhomogeneous, periodic in z deformations which tend to segregate it into segments of length $\lambda = 2\pi/\kappa$. Of course, this linear analysis is only valid as long as the perturbations are small, and so it does not imply that the vortex will actually break into segments – such a possibility is unlikely in view of the current conservation. Since the current density becomes inhomogeneous, this produces local inhomogeneities in the electric charge distribution in the form of a periodic sequence of positively and negatively charged regions along the vortex.

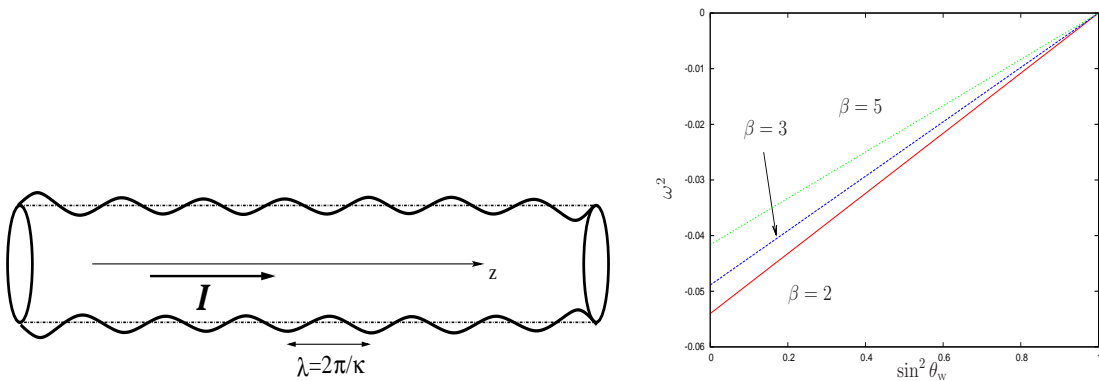


Figure 8: The effect of a proper negative mode on the vortex (left), and the eigenvalue $\omega^2(0)$ of the homogeneous perturbation mode versus θ_w for fixed $f_2(0) = 0.1$ (right).

The generic vortex perturbation can be decomposed into a sum over eigenmodes. As time increases, one can expect this sum to become dominated by negative modes whose growth rate is maximal (provided that the perturbation remains small). As is seen in Fig.4, $|\omega(\kappa)|$ is maximal for $\kappa = \pm\kappa_{\min}$ if $\mathcal{I} < \mathcal{I}_*$ and for $\kappa = 0$ if $\mathcal{I} > \mathcal{I}_*$. Therefore, for small currents the vortex will probably tend to segregate into segments of length $2\pi/\kappa_{\min}$ while for large currents it will rather expand homogeneously.

Since the wavevector of all negative modes is bounded, $|\kappa| < \kappa_{\max}$, their wavelength is larger than $2\pi/\kappa_{\max}$. Therefore, imposing periodic boundary conditions with period $2\pi/\kappa_{\max}$ will remove all these modes, because the vortex segment will not have enough room to accommodate them. Only the $\kappa = 0$ will stay, since it does not depend on z and so can be considered as periodic with any period. This poses no problems if $\mathcal{I} = 0$, or if $\mathcal{I} \neq 0$ but $\theta_w = \pi/2$, since this mode is non-negative in these cases. However, for $\theta_w < \pi/2$ and $\mathcal{I} \neq 0$ the homogeneous mode is negative. This is seen in Fig.4, in Table I, and also in Fig.8 which shows that $\omega^2(0)$ is negative for $\mathcal{I} \neq 0$ and vanishes only for $\theta_w = \pi/2$. This means that the generic vortices cannot be stabilized by periodic boundary conditions.

We did not find any simple arguments explaining why $\omega^2(0)$ should generically be negative. Since $\omega^2(0) = 0$ for $\theta_w = \pi/2$, when the massless fields decouple, one can suspect that the explanation could be related to the presence of the long-range field in the system. However, the massless fields decouple also for $\theta_w = 0$, but in this case one has $\omega^2(0) < 0$ (see Fig.8). It is therefore likely that the explanation should rather be related to the non-Abelian nature of the background solutions. Indeed, the non-linear commutator terms are generically present in the backgrounds, but they vanish for $\theta_w = \pi/2$ (when the SU(2) field decouples) or for $\mathcal{I} = 0$ (because Z strings are embedded Abelian solutions), that is exactly when $\omega^2(0)$ vanishes.

We have tried to analytically evaluate $\omega^2(0)$ for small currents by using the method applied in Ref. [23]. In this method both the background and perturbation equations are expanded in powers of the small parameter $q = f_2(0)$ and then solved order by order. We have found that $\omega^2(0) = -cq^2 + \dots$ where $c > 0$, so that the homogeneous mode becomes negative for however small currents. It is also negative for large currents, as is shown by (6.63). Therefore, it is generically negative.

Let us now consider electrically charged vortices with $I_0 \neq 0$. Since they can be obtained by boosting the $I_0 = 0$ vortex, their perturbation can also be obtained in the same way.

Boosting the proper modes (7.68) gives the negative modes (7.67) of the charged vortex, and we shall call such modes ‘boosted’ in order to distinguish them from the proper modes. The boosted modes grow not only in time but also in space, along the vortex, which is a simple consequence of the fact that the time/space directions for the boosted vortex are not the same as for the $I_0 = 0$ vortex. The proper negative modes of the latter grow only in time when considered in the restframe, but the observer comoving with the charged vortex will see the very same modes grow not only in time but also in space (see Fig.9). Equivalently, one can say that the boost renders complex the wavevector κ_b in (7.66), since ω is imaginary.

Since the boosted negative modes grow with z , they can be used only within a finite range of z for the small perturbation theory to be valid. This can be achieved by forming wavepackets. Let us consider a wavepacket of the proper eigenmodes of the $I_0 = 0$ vortex,

$$\delta f(t, \rho, z) = \int d\kappa C(\kappa) e^{i\omega(\kappa)t + i\kappa z} \Psi_\kappa(\rho) + \dots \quad (7.69)$$

where the dots stand for the contribution of the scattering states (solutions of (3.30) which do not vanish at infinity). Assuming the initial perturbation $\delta f(0, \rho, z)$ to have a compact

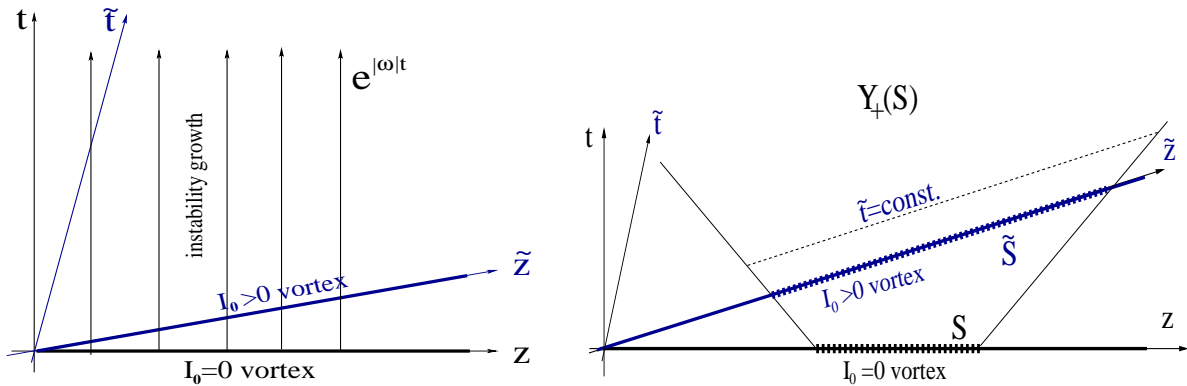


Figure 9: Left: The proper negative modes grow along the spacetime history lines. The restframe time of the $I_0 = 0$ vortex flows in the same direction, while for the boosted vortex the time direction is different so that the instability grows not only with time \tilde{t} but also with \tilde{z} . Right: Spacetime evolution of the initial data with compact support S .

support S along z -axis, its time evolution will be contained within the spacetime domain $Y_+(S)$ causally connected with S (see Fig.9). By simply changing the coordinates, $t = \cosh(b)\tilde{t} + \sinh(b)\tilde{z}$ and $z = \cosh(b)\tilde{z} + \sinh(b)\tilde{t}$, the same wave packet can be reexpressed

as sum over boosted modes,

$$\delta f(\tilde{t}, \rho, \tilde{z}) = \int d\kappa C(\kappa) e^{i\Xi(\tilde{t}, \tilde{z})} \Psi_\kappa(\rho) + \dots \quad (7.70)$$

where Ξ is given by (7.65)–(7.67). If there are negative modes in (7.69), then (7.70) will contain growing in \tilde{z} terms, but since \tilde{z} actually varies only within the finite range inside $Y_+(S)$ for a fixed \tilde{t} , the whole sum is bounded. One can therefore view this wavepacket as perturbation of the charged vortex with the initial distribution $\delta f(0, \rho, \tilde{z})$ contained in \tilde{S} (see Fig.9). If $\delta f(t, \rho, z)$ grows with t then $\delta f(\tilde{t}, \rho, \tilde{z})$ will grow with \tilde{t} , hence if the $I_0 = 0$ vortex is unstable then so is the $I_0 \neq 0$ vortex.

So far, however, the symmetry between the $I_0 = 0$ and $I_0 \neq 0$ vortices is incomplete, because we have found only the proper negative modes for the former and only the boosted negative modes for the latter. These modes were obtained by solving the radial equations (3.30) with real κ and real $\omega^2 < 0$ and they are spatially periodic in the vortex restframe but become non-periodic after the boost. One might therefore think that periodic boundary conditions could stabilize the charged vortices, since they will remove all boosted modes. However, there could be also solutions of Eqs.(3.30) giving rise to negative modes which are initially non-periodic but become periodic after the boost. The boosted value κ_b in (7.66) should then be real, hence one should look for bound state solutions of (3.30) for complex parameters

$$\omega = \gamma - i\Omega, \quad \kappa = K + i\Omega \tanh(b), \quad (7.71)$$

where $\gamma = \gamma(b, K)$, $\Omega = \Omega(b, K)$. It is worth noting that a similar recipe was considered within the stability analysis of the boosted black strings in the theory of gravity [28]. Inserting this in (7.66), the imaginary part of κ_b vanishes and one obtains

$$\exp(i\Xi) = \exp(\Omega_b t) \exp(i\gamma_b t + i\kappa_b z) \quad (7.72)$$

with

$$\Omega_b = \frac{\Omega t}{\cosh(b)}, \quad \gamma_b = \cosh(b)\gamma + \sinh(b)K, \quad \kappa_b = \cosh(b)K + \sinh(b)\gamma. \quad (7.73)$$

Since $\exp(i\Xi)$ grows in time and has the harmonic z -dependence, this corresponds to proper negative modes of the charged vortex with $I_0 = \mathcal{I} \sinh(b)$.

The next question is whether solutions of Eqs.(3.30) for the complex parameter values (7.71) exist. If $b = 0$ then κ is real and we should recover the already known solutions with

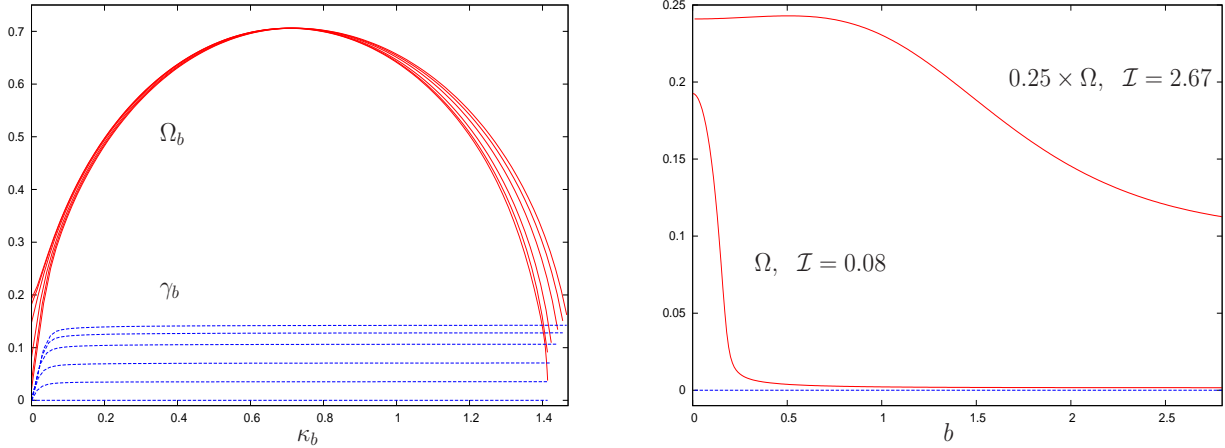


Figure 10: Left: Real and imaginary frequency parts γ_b and Ω_b versus κ_b for perturbations of the boosted vortex with $\mathcal{I} = 0.08$ for several values of the boost $b \in [0, 0.4]$. Right: Ω versus the boost parameter b for the homogeneous ($\kappa_b = 0$) perturbation mode for the boosted vortices with $\mathcal{I} = 0.08$ and $\mathcal{I} = 2.67$. In both panels $\beta = 2$, $\sin^2 \theta_W = 0.23$, $n = \nu = 1$, $m = 0$.

real $\omega^2 = -\Omega^2$, therefore one has $\gamma = 0$ in this case. If $b \neq 0$ then both ω^2 and κ become complex so that equations (3.30) should be complexified as well. We therefore obtain a system of 16 linear complex equations, which is equivalent to 32 real equations. This does not mean that the number of degrees of freedom doubles, since even for $b = 0$ we actually had $32(=40-8)$ real equations split into two independent subsystems of 16 equations each, equivalent to each other upon (3.21). For $b \neq 0$ we still have the 32 equations, but they no longer split into two subsystems.

Solving numerically the 32 coupled equations is considerably more time consuming than solving the 16 equations. This is why we did not carry out a systematic analysis of the parameter space but studied instead just several representative cases. We integrated the equations looking for bound state solutions with the boundary conditions given by the complexified version of (3.32),(3.33). Choosing a value of b , we have managed to explicitly construct such solutions and determine γ and Ω as functions of K .

It turns out that the dispersion relation for Ω_b against κ_b remains qualitatively the same for $b \neq 0$ as for $b = 0$ (see Fig.10). If the current \mathcal{I} is small and b is fixed then $\Omega(\kappa_b)$ starts at a non-zero value at $\kappa_b = 0$, increases and reaches maximum, then decreases and vanishes for some maximal value $\kappa_b = \kappa_{\max}$ (see Fig.10). For large currents $\Omega(\kappa_b)$ decreases monotonously from its value at $\kappa_b = 0$ till zero. One has $\Omega(\kappa_b) = \Omega(-\kappa_b)$.

The proper negative modes therefore exist for any value of charge and not only for $I_0 = 0$. To completely restore the symmetry between solutions with different I_0 , we note that the proper negative modes for any b can be boosted towards a different value of the boost parameter, B , say. This will give boosted negative modes of the $I_0 = \mathcal{I} \sinh(B)$ vortex proportional to

$$\exp \{ \Omega_b \cosh(B - b) t + \Omega_b \sinh(B - b) z \} \exp \{ i(\gamma_B t + \kappa_B z) \} \quad (7.74)$$

with $\kappa_B = \cosh(B)K + \sinh(B)\gamma$ and $\gamma_B = \cosh(B)\gamma + \sinh(B)K$. Therefore, for any vortex charge $I_0 = \mathcal{I} \sinh(B)$ there are proper negative modes, but also infinitely many boosted modes labeled by $b \neq B$. The space of negative modes has the same structure for any value of charge, since there is one-to-one correspondence between modes for different charges via boosts, as schematically shown in Fig.11.

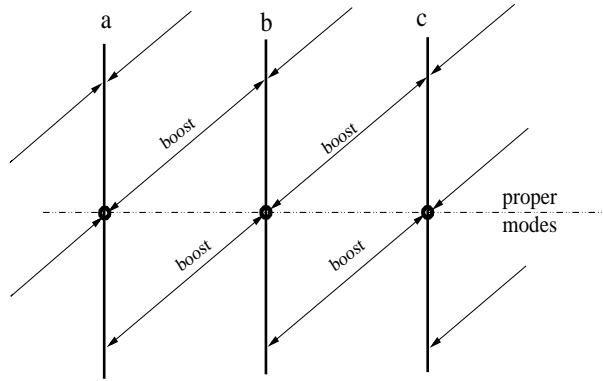


Figure 11: The set of negative modes for any given vortex charge, for example $I_0 = \mathcal{I} \cosh(b)$, is represented by the vertical line. The proper modes are represented by the fat points. There is one-to-one correspondence between modes for different I_0 via boosts.

The boosted negative modes are non-periodic in space and can contribute only to the instability of infinitely long vortices, but they will be removed by imposing on vortex the periodic boundary conditions. The proper modes will stay then, but if the period is less than $2\pi/\kappa_{\max}$ then they will be removed as well, apart from the $\kappa_b = 0$ mode. We know that for $I_0 = 0$ this mode is generically negative, but perhaps things may change for $I_0 \neq 0$? We therefore trace Ω for this mode against b and find that it decreases very rapidly with b , especially for small currents (see Fig.10), so that the instability growth rate decreases when the vortex charge I_0 increases. However, it is not clear from these data if Ω always

stays finite or eventually vanishes at some large value of b . It seems however that the latter option is impossible, since $\kappa_b = 0$ implies that $\gamma = K = 0$. Setting $\Omega = 0$ would therefore mean that $\omega = \kappa = 0$, but since $\kappa = 0$ is real, this solution should be contained in the previously obtained dispersion relation $\omega^2(\kappa)$. However, we know from the previous analysis that $\omega^2 \neq 0$ for $\kappa = 0$ (unless $\mathcal{I} = 0$), and so the value $\Omega = 0$ is impossible. Therefore, there is no critical value of boost for which the homogeneous instability would disappear.

VIII. CONCLUSIONS

We study in this paper the stability of the superconducting vortex solutions in the Weinberg-Salam theory described in Ref. [12]. Such vortices are characterized by a constant electric current $I_3 = \mathcal{I} \cosh(b)$ and linear electric charge density $I_0 = \mathcal{I} \sinh(b)$ comprising a spacelike vector (I_0, I_3) . Fixing \mathcal{I} , vortices with different values of the charge I_0 can be related to each other by Lorentz boosts, in particular there exists the restframe where $I_0 = 0$. For $\mathcal{I} \rightarrow 0$ all solutions become Z strings, while for $\theta_w \rightarrow \pi/2$ and $\beta > 1$ they reduce to the twisted semilocal strings studied in Ref. [24].

We consider generic vortex perturbations in the linear approximation and find that after separating the variables the perturbation equations reduce to the effective 16-channel Schrödinger problem (3.30). This problem admits bound state solutions with $\omega^2 < 0$ whose dispersion relation $\omega^2(\kappa)$ is shown in Fig.4 and tabulated in Table I. These solutions describe the ‘proper’ negative modes of the $I_0 = 0$ vortex. Choosing the parameters ω, κ in Eqs.(3.30) to be complex gives bound state solutions describing proper negative modes of the charged vortices. As a result, for any given value of charge I_0 there is a one-parameter family of proper negative modes which can be labeled by the wavevector κ_b . These perturbation modes grow in time favoring segregation of the homogeneous vortex into segments, although one cannot conclude from the perturbative analysis whether it will actually break in pieces in the long run.

Since vortices with different I_0 are related by Lorentz boosts, their perturbations can be related in this way too. Boosting the proper negative modes of the $I_0 = \mathcal{I} \sinh(b)$ vortex one obtains negative modes of the $I_0 = \mathcal{I} \sinh(B)$ vortex, so that the latter acquires in fact an additional infinity of negative modes labeled by $b \neq B$. These ‘boosted’ modes grow with z but they can form localized wavepackets to contribute to the instability of infinitely long

vortices. Since they are non-periodic in space, they can be removed by imposing periodic boundary conditions along the vortex.

The proper negative modes are proportional to $\exp\{i\kappa_b z\}$ and so they can be made compatible with the periodicity along z by adjusting the value of κ_b . However, they exist only for $|\kappa_b| < \kappa_{\max}$ and so choosing the period to be less than $2\pi/\kappa_{\max}$ the vortex segment will not have enough room to accommodate these modes. All of them will therefore be removed, apart from the $\kappa_b = 0$ mode which is independent of z and can be considered as periodic with any period. Therefore, the only remaining vortex instability is associated with this homogeneous mode.

In some cases one has $\omega = 0$ for $\kappa_b = 0$, as for example for $\theta_w = \pi/2$ and for any \mathcal{I} (semilocal vortices), or for $\mathcal{I} = 0$ and for any θ_w (Z strings). In these cases the homogeneous mode is not negative and so the short periodic vortex segments turn out to be stable. In particular, Z strings can be stabilized in this way by passing to the gauge (5.50) and then imposing the periodic boundary conditions which break the gauge invariance. However, in the generic case the homogeneous mode is negative and it renders the vortex unstable with respect to the homogeneous expansion even after imposing periodic boundary conditions.

At the same time, it is possible that the homogeneous negative mode could be removed by the curvature effects. Specifically, let us suppose that one ‘cuts out’ a finite vortex segment, bends it and identifies its extremities to make a loop. Then, since the loop thickness cannot be larger than its radius, the homogeneous expansion of the vortex segment should inevitably stop at some point. Therefore, the homogeneous instability will be removed, suggesting that the loop could be stable. Of course, this argument is only qualitative. Moreover, new instabilities could appear when bending the vortex. However, any possibility to have stable electroweak solitons, as for example vortex loops, could be very important. Such loops could be balanced against contraction by the centrifugal force arising from the momentum circulating along them. Since momentum flows along vortices with $I_0 \neq 0$, they can be naturally used to ‘make’ the loops. All this suggests that spinning vortex loops – electroweak analogs of the ‘cosmic vortons’ [25] – could exist and could perhaps even be stable. Of course, verification of this conjecture requires serious efforts, since so far vortons have been explicitly constructed only in a simple scalar field model [26], [27]. However, if the electroweak vortons indeed exist and are stable, they could be a dark matter candidate.

There could be other physical manifestations of the superconducting vortices. They could

perhaps be created either at high temperatures or in high energy collisions, and since they are non-topological, they could exist in the form of finite segments. If their extremities are attached to something (charged clouds), then they could be spatially periodic and transfer charge between different regions of space like ‘electroweak thunderbolts’. Non-periodic vortex segments should decay emitting jets of W^\pm through its extremities, which could perhaps be detectable at the LHC. Specifically, large magnetic fields similar to those inside the vortex and also large currents can be created in the LHC heavy ion collisions. This could lead to creation of virtual vortex segments whose subsequent disintegration would be accompanied by showers of W^\pm 's. As a result, if one observes an excessive W^\pm production in the collisions, this could indicate the vortex segment creation. A similar way to detect the presence of the non-perturbative electroweak structures in the LHC collisions was discussed in [29].

ACKNOWLEDGEMENTS

We would like to thank Jan Ambjorn, Christos Charmousis, Maxim Chernodub, Tom Kibble, Frans Klinkhamer, Alexey Morozov, Niels Obers, Paul Olesen, Eugen Radu, Mikhail Shaposhnikov, Sergey Solodukhin, Toby Wiseman, and Andreas Wipf for discussions and remarks at various stages of this work.

APPENDIX A. BACKGROUND FIELD EQUATIONS

With the parametrization (2.9) the field equations (2.3)–(2.5) reduce to two U(1) equations (with $' \equiv \frac{d}{d\rho}$)

$$\frac{1}{\rho}(\rho u')' = \frac{g'^2}{2} \left\{ (u + u_3)f_1^2 + 2u_1f_1f_2 + (u - u_3)f_2^2 \right\}, \quad (\text{A.1})$$

$$\rho \left(\frac{v'}{\rho} \right)' = \frac{g'^2}{2} \left\{ (v + v_3)f_1^2 + 2v_1f_1f_2 + (v - v_3)f_2^2 \right\}, \quad (\text{A.2})$$

two Higgs equations

$$\begin{aligned} \frac{1}{\rho}(\rho f_1')' &= \left\{ \frac{\sigma^2}{4} [(u + u_3)^2 + u_1^2] + \frac{1}{4\rho^2} [(v + v_3)^2 + v_1^2] + \frac{\beta}{4}(f_1^2 + f_2^2 - 1) \right\} f_1 \\ &+ \left(\frac{\sigma^2}{2} uu_1 + \frac{1}{2\rho^2} vv_1 \right) f_2, \end{aligned} \quad (\text{A.3})$$

$$\begin{aligned} \frac{1}{\rho}(\rho f_2')' &= \left\{ \frac{\sigma^2}{4} [(u - u_3)^2 + u_1^2] + \frac{1}{4\rho^2} [(v - v_3)^2 + v_1^2] + \frac{\beta}{4}(f_1^2 + f_2^2 - 1) \right\} f_2 \\ &+ \left(\frac{\sigma^2}{2} uu_1 + \frac{1}{2\rho^2} vv_1 \right) f_1, \end{aligned} \quad (\text{A.4})$$

four Yang-Mills equations

$$\frac{1}{\rho}(\rho u_1')' = -\frac{1}{\rho^2} (v_1 u_3 - v_3 u_1) v_3 + \frac{g^2}{2} [u_1(f_1^2 + f_2^2) + 2u f_1 f_2], \quad (\text{A.5})$$

$$\frac{1}{\rho}(\rho u_3')' = +\frac{1}{\rho^2} (v_1 u_3 - v_3 u_1) v_1 + \frac{g^2}{2} [(u_3 + u)f_1^2 + (u_3 - u)f_2^2], \quad (\text{A.6})$$

$$\rho \left(\frac{v_1'}{\rho} \right)' = +\sigma^2 (v_1 u_3 - v_3 u_1) u_3 + \frac{g^2}{2} [v_1(f_1^2 + f_2^2) + 2v f_1 f_2], \quad (\text{A.7})$$

$$\rho \left(\frac{v_3'}{\rho} \right)' = -\sigma^2 (v_1 u_3 - v_3 u_1) u_1 + \frac{g^2}{2} [(v_3 + v)f_1^2 + (v_3 - v)f_2^2], \quad (\text{A.8})$$

and a first order constraint

$$\sigma^2 (u_1 u_3' - u_3 u_1') + \frac{1}{\rho^2} (v_1 v_3' - v_3 v_1') - g^2 (f_1 f_2' - f_2 f_1') = 0. \quad (\text{A.9})$$

APPENDIX B. PERTURBATION EQUATIONS

Fixing the gauge, decoupling the ghost modes as described in the main text and using the parametrization (3.28) for perturbations in the physical sector, the perturbation equations can be written in the form of the 16-channel Schrödinger problem

$$-\frac{1}{\rho}(\rho\Psi')' + \mathcal{U}\Psi = \omega^2\Psi, \quad (\text{B.1})$$

where the 16-component vector Ψ and the 16 symmetric potential matrix \mathcal{U} read

$$\Psi = \begin{pmatrix} \vec{Z} \\ \vec{\mathcal{A}} \\ \vec{\mathcal{W}}^+ \\ \vec{\mathcal{W}}^- \\ \vec{\mathcal{H}} \end{pmatrix}, \quad \mathcal{U} = \begin{pmatrix} \Delta_Z & \Gamma_{ZA} & \Gamma_{ZW^+} & \Gamma_{ZW^-} & \Gamma_{ZH} \\ \Gamma_{ZA} & \Delta_A & \Gamma_{AW^+} & \Gamma_{AW^-} & \Gamma_{AH} \\ \Gamma_{ZW^+} & \Gamma_{AW^+} & \Delta_{W^+} & \Gamma_{WW} & \Gamma_{W^+\mathcal{H}} \\ \Gamma_{ZW^-} & \Gamma_{AW^-} & \Gamma_{WW} & \Delta_{W^-} & \Gamma_{W^-\mathcal{H}} \\ \Gamma_{ZH} & \Gamma_{AH} & \Gamma_{W^+\mathcal{H}} & \Gamma_{W^-\mathcal{H}} & \Delta_{\mathcal{H}} \end{pmatrix}. \quad (\text{B.2})$$

Here

$$\vec{z} = \begin{pmatrix} z_0 \\ z_+ \\ z_- \end{pmatrix}, \quad \vec{A} = \begin{pmatrix} A_0 \\ A_+ \\ A_- \end{pmatrix}, \quad \vec{W}^\pm = \begin{pmatrix} W_0^\pm \\ W_+^\pm \\ W_-^\pm \end{pmatrix}, \quad \vec{H} = \begin{pmatrix} h_1^+ \\ h_1^- \\ h_2^+ \\ h_2^- \end{pmatrix}, \quad (\text{B.3})$$

and $\Delta_z = \text{diag}(\Delta_0^z, \Delta_{+1}^z, \Delta_{-1}^z)$ also $\Delta_A = \text{diag}(\Delta_0^A, \Delta_{+1}^A, \Delta_{-1}^A)$ while

$$\Delta_{W^\pm} = \begin{pmatrix} \Delta_0^{W^\pm} & \pm Q & \pm Q \\ \pm Q & \Delta_{+1}^{W^\pm} & 0 \\ \pm Q & 0 & \Delta_{-1}^{W^\pm} \end{pmatrix}, \quad \Delta_{\mathcal{H}} = \begin{pmatrix} \Delta_{+1}^{h_1} & V_1 & V_+ & V_0 \\ V_1 & \Delta_{-1}^{h_1} & V_0 & V_- \\ V_+ & V_0 & \Delta_{+1}^{h_2} & V_2 \\ V_0 & V_- & V_2 & \Delta_{-1}^{h_2} \end{pmatrix} \quad (\text{B.4})$$

with ($\eta = 0, \pm 1$)

$$\begin{aligned} \Delta_\eta^z &= \frac{g^2 v_1^2 + (m - \eta)^2}{\rho^2} + g^2 \sigma^2 u_1^2 + \kappa^2 + \frac{1}{2}(f_1^2 + f_2^2) - 2g^2 g'^2 f_2^2, \\ \Delta_\eta^A &= \frac{g'^2 v_1^2 + (m - \eta)^2}{\rho^2} + g'^2 \sigma^2 u_1^2 + \kappa^2 + 2g^2 g'^2 f_2^2, \\ \Delta_\eta^{W^\pm} &= \frac{v_1^2/2 + (v_3 \pm (m - \eta))^2}{\rho^2} \pm 2\eta \frac{v_3'}{\rho} + \frac{\sigma^2 u_1^2}{2} + (\sigma u_3 \mp \kappa)^2 + \frac{g^2}{2}(f_1^2 + f_2^2), \\ \Delta_\pm^{h_1} &= \frac{v_1^2/4 + \left(\frac{v+v_3}{2} \mp m\right)^2}{\rho^2} + \left(\frac{\sigma u_1}{2}\right)^2 + \left(\frac{\sigma}{2}(u + u_3) \pm \kappa\right)^2 + \frac{\beta}{4}(2f_1^2 + f_2^2 - 1) \\ &\quad + \frac{f_1^2}{4} + \frac{g^2 f_2^2}{2}, \\ \Delta_\pm^{h_2} &= \frac{v_1^2/4 + \left(\frac{v-v_3}{2} \mp m\right)^2}{\rho^2} + \left(\frac{\sigma u_1}{2}\right)^2 + \left(\frac{\sigma}{2}(u - u_3) \pm \kappa\right)^2 + \frac{\beta}{4}(f_1^2 + 2f_2^2 - 1) \\ &\quad + \frac{f_2^2}{4} + \frac{g^2 f_1^2}{2}, \\ Q &= -\sqrt{2}\sigma u_3', \quad V_{1,2} = (1 - \beta)\frac{f_{1,2}^2}{4}, \quad V_0 = (1 - \beta)\frac{f_1 f_2}{4}, \\ V_\pm &= \frac{v_1}{\rho^2} \left(\frac{v}{2} \mp m\right) + \sigma u_1 \left(\frac{\sigma u}{2} \pm \kappa\right) + (g'^2 - g^2 + \beta)\frac{f_1 f_2}{4}. \end{aligned} \quad (\text{B.5})$$

The vector-vector couplings are defined by

$$\Gamma_{xy} = \begin{pmatrix} d_0^{xy} & e_{+1}^{xy} & e_{-1}^{xy} \\ e_{-1}^{xy} & d_{+1}^{xy} & 0 \\ e_{+1}^{xy} & 0 & d_{-1}^{xy} \end{pmatrix}, \quad (\text{B.6})$$

where x and y design \mathcal{Z} , \mathcal{A} , \mathcal{W}^+ , \mathcal{W}^- and

$$\begin{aligned} d_\eta^{\mathcal{Z}\mathcal{A}} &= -gg' \left(\frac{v_1^2}{\rho^2} + \sigma^2 u_1^2 + (g^2 - g'^2) f_2^2 \right), & d_\eta^{\mathcal{W}\mathcal{W}} &= -\frac{1}{2} \left(\frac{v_1^2}{\rho^2} + \sigma^2 u_1^2 \right), \\ d_\eta^{\mathcal{Z}\mathcal{W}^\pm} &= -g\sqrt{2} \left(\pm\eta \frac{v_1'}{\rho} + \frac{v_1}{\rho^2} \left(\frac{v_3}{2} \pm (m - \eta) \right) + \sigma u_1 \left(\frac{\sigma u_3}{2} \mp \kappa \right) - \frac{g'^2}{2} f_1 f_2 \right), \\ d_\eta^{\mathcal{A}\mathcal{W}^\pm} &= g'\sqrt{2} \left(\pm\eta \frac{v_1'}{\rho} + \frac{v_1}{\rho^2} \left(\frac{v_3}{2} \pm (m - \eta) \right) + \sigma u_1 \left(\frac{\sigma u_3}{2} \mp \kappa \right) + \frac{g^2}{2} f_1 f_2 \right), \end{aligned} \quad (\text{B.7})$$

while

$$\begin{aligned} e_\eta^{\mathcal{Z}\mathcal{W}^\pm} &= \pm g \left(\sigma u_1' \pm \eta \frac{\sigma}{\rho} (v_3 u_1 - v_1 u_3) \right), & e_\eta^{\mathcal{Z}\mathcal{A}} &= 0, \\ e_\eta^{\mathcal{A}\mathcal{W}^\pm} &= \mp g' \left(\sigma u_1' \pm \eta \frac{\sigma}{\rho} (v_3 u_1 - v_1 u_3) \right), & e_\eta^{\mathcal{W}\mathcal{W}} &= 0. \end{aligned} \quad (\text{B.8})$$

Finally, the vector-scalar couplings are

$$\begin{aligned} \Gamma_{\mathcal{Z}\mathcal{H}} &= \begin{pmatrix} -a_1^0 & a_1^0 & (g^2 - g'^2)a_2^0 & (g'^2 - g^2)a_2^0 \\ a_1^+ & a_1^- & (g'^2 - g^2)a_2^+ & (g'^2 - g^2)a_2^- \\ a_1^- & a_1^+ & (g'^2 - g^2)a_2^- & (g'^2 - g^2)a_2^+ \end{pmatrix}, & \Gamma_{\mathcal{A}\mathcal{H}} &= 2gg' \begin{pmatrix} 0 & 0 & -a_2^0 & a_2^0 \\ 0 & 0 & a_2^+ & a_2^- \\ 0 & 0 & a_2^- & a_2^+ \end{pmatrix}, \\ \Gamma_{\mathcal{W}^+\mathcal{H}} &= g\sqrt{2} \begin{pmatrix} 0 & a_2^0 & -a_1^0 & 0 \\ 0 & a_2^- & a_1^+ & 0 \\ 0 & a_2^+ & a_1^- & 0 \end{pmatrix}, & \Gamma_{\mathcal{W}^-\mathcal{H}} &= g\sqrt{2} \begin{pmatrix} -a_2^0 & 0 & 0 & a_1^0 \\ a_2^+ & 0 & 0 & a_1^- \\ a_2^- & 0 & 0 & a_1^+ \end{pmatrix}, \end{aligned} \quad (\text{B.9})$$

where

$$\begin{aligned} a_1^0 &= \frac{\sigma}{2} ((u + u_3)f_1 + u_1 f_2), & a_2^0 &= \frac{\sigma}{2} ((u - u_3)f_2 + u_1 f_1), \\ a_1^\pm &= \frac{1}{\sqrt{2}} \left(f_1' \pm \frac{1}{2\rho} ((v + v_3)f_1 + v_1 f_2) \right), & a_2^\pm &= \frac{1}{\sqrt{2}} \left(f_2' \pm \frac{1}{2\rho} ((v - v_3)f_2 + v_1 f_1) \right). \end{aligned} \quad (\text{B.10})$$

-
- [1] E. Witten, *Superconducting strings*. *Nucl.Phys.* **B249** (1985) 557.
[2] A.A. Abrikosov, *On the magnetic properties of superconductors of the second group*. *Sov.Phys. JETP* **5** (1957) 1174; H.B. Nielsen and P. Olesen, *Vortex line models for dual strings*. *Nucl.Phys.* **B61** (1973) 45.
[3] A. Babul, T. Piran and D.N. Spergel, *Bosonic superconducting cosmic strings. 1. Classical Field Theory solutions*. *Phys.Lett.* **B202** (1988) 307; R.L. Davis and E.P.S. Shellard, *The*

- physics of vortex superconductivity. Phys.Lett.* **B207** (1988) 404; C.T. Hill, H.M. Hodges and M.S. Turner, *Bosonic superconducting cosmic strings. Phys.Rev.* **D37** (1988) 263; P. Amsterdamski and P. Laguna-Castillo, *Internal structure of superconducting bosonic strings. Phys.Rev.* **D37** (1988) 877; D. Haws, M. Hindmarsh and N. Turok, *Superconducting strings or springs ? Phys.Lett.* **B209** (1988) 255; P. Peter, *Superconducting cosmic strings: Equation of state for spacelike and timelike current in the neutral limit. Phys.Rev.* **D45** (1991) 1091.
- [4] B. Carter, *Duality relation between charged elastic strings and superconducting cosmic strings. Phys.Lett.* **B224** (1989) 61; *Stability and characteristic propagation speed in superconducting cosmic and other string models. Phys.Lett.* **B228** (1989) 466.
- [5] A. Vilenkin and E.P.S. Shellard, *Cosmic strings and other topological defects.* Cambridge University Press, Cambridge (1994).
- [6] M. Hindmarsh and T.W.B. Kibble, *Cosmic strings. Rep.Prog.Phys.* **58** (1995) 477.
- [7] T. Vachaspati, *Vortex solutions in the Weinberg-Salam model. Phys.Rev.Lett.* **68** (1992) 1977; A.Achucarro and T. Vachaspati, *Semilocal and electroweak strings. Phys.Rep.* **327** (2000) 427.
- [8] W. B. Perkins, *W condensation in electroweak strings. Phys.Rev.* **D47** (1993) R5224.
- [9] P. Olesen, *A W dressed electroweak string. hep-ph/9310275.*
- [10] A. Achucarro, R. Gregory, J.A. Harvey and K. Kuijken, *Role of W condensation in electroweak string stability. Phys.Rev.Lett.* **72** (1994) 3646.
- [11] M.S. Volkov, *Superconducting electroweak strings. Phys.Lett.* **B644** (2007) 203.
- [12] J. Garaud and M.S. Volkov, *Superconducting non-Abelian vortices in Weinberg-Salam theory – electroweak thunderbolts. Nucl.Phys.* **B826** (2010) 174.
- [13] M. Goodband and M. Hindmarsh. *Instabilities of electroweak strings. Phys.Lett.* **B363** (1995) 58; M. Goodband and M. Hindmarsh. *Bound states and instabilities of vortices. Phys.Rev.* **D52** (1995) 4621.
- [14] M. James, L. Perivolaropoulos, T. Vachaspati, *Detailed stability analysis of electroweak strings. Nucl.Phys.* **B395** (1993) 534.
- [15] F.R. Klinkhamer and P. Olesen, *A new perspective on electroweak string. Nucl.Phys.* **B422** (1994) 227.
- [16] J. Garaud and M.S. Volkov, *Stability analysis of the twisted superconducting semilocal strings. Nucl.Phys.* **B799** (2008) 430.

- [17] J. Eggers, *Nonlinear dynamics and breakup of free-surface flows*. *Rev.Mod.Phys.* **69** (1997) 865; T. Harmark, V. Niarchos and N.A. Obers. *Instabilities of black strings and branes*. *Class.Quant.Grav.* **24** (2007) R1.
- [18] Y. Nambu, *Stringlike configurations in the Weinberg-Salam theory*. *Nucl.Phys.* **B130** (1977) 505.
- [19] J. Ambjorn and P. Olesen, *On the electroweak magnetism*. *Nucl.Phys.* **B315** (1989) 606; *A condensate solution of the electroweak theory which interpolates between the broken and the symmetric phase*. *Nucl.Phys.* **B330** (1990) 193; *Electroweak magnetism: theory and applications*. *Int.Journ.Mod.Phys.* **A5** (1990) 4525.
- [20] I.M. Gel'fand and S.V. Fomin, *Calculus of variations*. Prentice Hill, Englewood Cliffs (1963).
- [21] H. Amann, P. Quittner, *A nodal theorem for coupled systems of Schrödinger equations and the number of bound states*. *J.Math.Phys.* **36** (1995) 4553.
- [22] J. Stoer, R. Bulirsch, *Introduction to numerical analysis*. Springer, New York (2002).
- [23] P. Forgacs and A. Lukacs, *Instabilities of twisted vortices*. *JHEP* **0912** (2009) 064.
- [24] P. Forgacs, S. Reuillon, M.S. Volkov, *Superconducting vortices in semilocal models*. *Phys.Rev.Lett.* **96** (2006) 041601; *Twisted superconducting semilocal strings*. *Nucl.Phys.* **B751** (2006) 390.
- [25] R.L. Davis and E.P.S. Shellard. *Cosmic vortons*. *Nucl.Phys.* **B323** (1993) 209.
- [26] E. Radu and M.S. Volkov. *Stationary ring solitons in field theory – knots and vortons*. *Phys.Rep.* **468** (2008) 101.
- [27] R. Battye and P.M. Sutcliffe. *Vorton construction and dynamics*. *Nucl.Phys.* **B814** (2009) 180.
- [28] J.L. Hovdebo and R.C. Myers. *Black rings, boosted strings, and Gregory-Laflamme instability*. *Phys.Rev.* **D 73** (2006) 084013.
- [29] J. Ambjorn and P. Olesen. *W condensate formation in high-energy collisions*. *Phys.Lett.* **B257** (1991) 201.